Summer 8-14-2020

Cooperativity of CCNE1 and FOXM1 in High-Grade Serous Ovarian Cancer

Lucy Elge
University of Nebraska Medical Center

COOPERATIVITY OF CCNE1 AND FOXM1 IN HIGH-GRADE SEROUS OVARIAN CANCER

by

Lucy Elge

A THESIS

Presented to the Faculty of
the University of Nebraska Graduate College
in Partial Fulfillment of the Requirements
for the Degree of Master of Science

Cancer Research Graduate Program

Under the Supervision of Professor Adam R. Karpf

University of Nebraska Medical Center
Omaha, Nebraska

July 2020

Supervisory Committee:

Keith Johnson, Ph.D.

Jennifer Black, Ph.D.

ACKNOWLEDGEMENTS

First, I must express my gratitude for Dr. Adam R. Karpf, for without his support and mentorship this project would not have been possible. Under his guidance, I learned tenacity and independent critical thinking which will serve me well in future endeavors. I'd also like to acknowledge the past and present members of the Karpf lab: Connor Branick, Lidia Boghean, Catalina Muñoz, and Cassie Liu. Our lively discussions always broadened my thinking and encouraged me to think intensively about the issues at hand. Their patience and collaboration in the lab was instrumental in my development, and their friendship has proved to be invaluable.

I want to thank my supervisory committee members: Dr. Keith Johnson and Dr. Jennifer Black. Their input and encouragement helped foster my growth as a scientist and improved the quality of my project immensely. Additionally, I would like to thank Dr. Jixin Dong for serving on my comprehensive exam committee.

I'd like to acknowledge all collaborators for their contribution of reagents, including Dr. Jixin Dong and Dr. Amar Natarajan.

For the conducive learning environment, I'd like to thank the Eppley Institute, Cancer Research Program, and Graduate Studies.

Finally, I would be remiss without acknowledging my husband Tyler, my family and my faith, for without their support, absolutely none of this would be possible. Soli Deo gloria.

COOPERATIVITY OF CCNE1 AND FOXM1 IN HIGH-GRADE SEROUS OVARIAN CANCER

Lucy G. Elge, M.S.

University of Nebraska Medical Center, 2020

Supervisor: Adam R. Karpf, Ph.D.

High-grade serous ovarian cancer (HGSC) ranks as the fifth leading cause of female cancer related deaths. A greater understanding of the molecular mechanisms underlying HGSC will elucidate better detection methods and identify potential treatment targets.

Forkhead Box M1 (FOXM1) is a key player in HGSC, as data from The Cancer Genome Atlas (TCGA) revealed that its activation is the second most frequent molecular alteration in HGSC. Similarly, cyclin E1 (CCNE1) is also important in HGSC, as the gene is amplified in 20% of HGSC cases. Both genes and proteins have been studied extensively, but the potential interaction between the two has not been examined in HGSC progression or in other cancer models.

We found that dual ectopic expression of CCNE1 and FOXM1 leads to phosphorylation of FOXM1 in a HGSC cell precursor model [fallopian tube epithelial (FTE) cells] at residue threonine 600, contributing to activation of FOXM1. Our studies reveal that the reaction is mediated primarily through the CCNE1 and cyclin dependent kinase (CDK) 2 complex. Importantly, transformation assays revealed that CCNE1 and FOXM1 contribute to FTE cell proliferation, migration, and invasion in a cooperative manner.

Further evidence for a functional interaction between CCNE1 and FOXM1 was

observed in HGSC lines. Phosphorylated FOXM1 (p-FOXM1) was found in HGSC cell lines and primary epithelial ovarian carcinoma (EOC) tumor samples. In primary EOC tumor samples, CCNE1, FOXM1, and CDK2 correlate strongly with p-FOXM1 expression. Treatment with a CDK2 inhibitor, dinaciclib, resulted in a marked decrease of p-FOXM1 in a FTE and HGSC model, validating CDK2 as a critical factor in FOXM1 phosphorylation.

TABLE OF CONTENTS

LIST OF FIGURES

LIST OF TABLES

LIST OF ABBREVIATIONS

BER	Base excision repair
CA125	Carbohydrate 125 antigen
CCNE1	Cyclin E1
CDK1	Cyclin dependent kinase 1
CDK2	Cyclin dependent kinase 2
CDKi	Cyclin dependent kinase inhibitor
CDT1	Chromosome licensing and DNA replication factor 1
CE	Cytoplasmic extract
CNA	Copy number alterations
DBD	DNA binding domain
DNA	Deoxyribonucleic Acid
Dox	Doxycycline
DRS	DNA replication stress
EOC	Epithelial ovarian cancer
ESP	Early serous proliferation
FOXM1	Forkhead box M1
FT282	Immortalized FTE cell line from patient donor #282
FTE	Fallopian tube epithelium
HE4	Human epididymal secretory protein E4
HGSC	High-grade serous ovarian cancer
HR	Homologous recombination DNA repair
LMW	Low molecular weight
MCM2	Minichromosome maintenance complex component 2
MEF	Mouse embryonic fibroblasts
MPP-2	M-phase phosphoprotein 2, a.k.a. FOXM1

mRNA	Messenger ribonucleic acid
NCI	National Cancer Institute
NE	Nuclear extract
NHEJ	Non-homologous end joining
NO	Normal ovary
NRD	N-terminal repressor domain
OC	Ovarian cancer
OSE	Ovarian surface epithelium
p-FOXM1	Phosphorylated forkhead box M1 protein
PARPi	Poly ADP ribose polymerase inhibitor
RNA	Ribonucleic acid
SDS	Sodium dodecyl sulfate
STIC	Serous tubal intraepithelial carcinoma
TAD	Transactivation domain
TCGA	The Cancer Genome Atlas
TF	Transcription factor
TVS	Transvaginal sonography
UTR	Untranslated region
WHO	World Health Organization
WT	Wild typ

CHAPTER 1: INTRODUCTION

HUMAN OVARIAN CANCER

Overview of ovarian cancer

Ovarian cancer has been termed a “silent killer” of women, as it is the most lethal cancer of the female reproductive system and often occurs without definitive symptoms. The National Cancer Institute (NCI) estimates that there will be 21,750 new ovarian cancer cases in 2020, accounting for 1.2% of all new cancer cases in the United States (1). While ovarian cancer may not rank high in terms of prevalence, it is decidedly lethal. Ovarian cancer is projected to claim the lives of 13,940 women this year, making it the fifth leading cancer related cause of death for women (1).

The overall 5 year survival rate for women diagnosed with ovarian cancer is 48.6%, but when parsed out to localized versus metastatic disease, the 5 year survival rate tells a startling story (1). If the cancer remains localized to the ovaries, the 5 year survival rate is over 90%. Alternatively, if the disease has spread beyond the ovaries, the 5 year survival rate drops drastically, to less than 30%. The majority of ovarian cancer patients (over 60%) are diagnosed after cancer cells have metastasized; thus many ovarian cancer patients find themselves facing a dismal survival rate (2). These statistics underscore the need for more effective early screening and emphasize the difficulty of successful treatment of advanced stage disease.

Ovarian cancer is a generic term for a heterogeneous set of neoplasms that localize to the ovaries. Based on the cell of origin, ovarian cancer is classified into three major categories: epithelial, germ cell, and stromal cell derived tumors. Of these types, epithelial ovarian cancer (EOC) is the predominant in terms of prevalence, accounting for around 90% of ovarian cancers (3). Furthermore, EOC can be sub-categorized based on histology, utilizing a system devised by the World Health Organization (WHO) (4, 5).

There are five histological EOC subtypes: high-grade serous, endometrioid, mucinous, clear-cell, and low-grade serous (Figure 1). These subtypes differ in their tissue of origin, pathogenesis, molecular alterations, risk factors, and overall prognosis. High-grade serous ovarian cancer (HGSC) is by far the most common subtype, comprising 70% of EOC (7, 8).

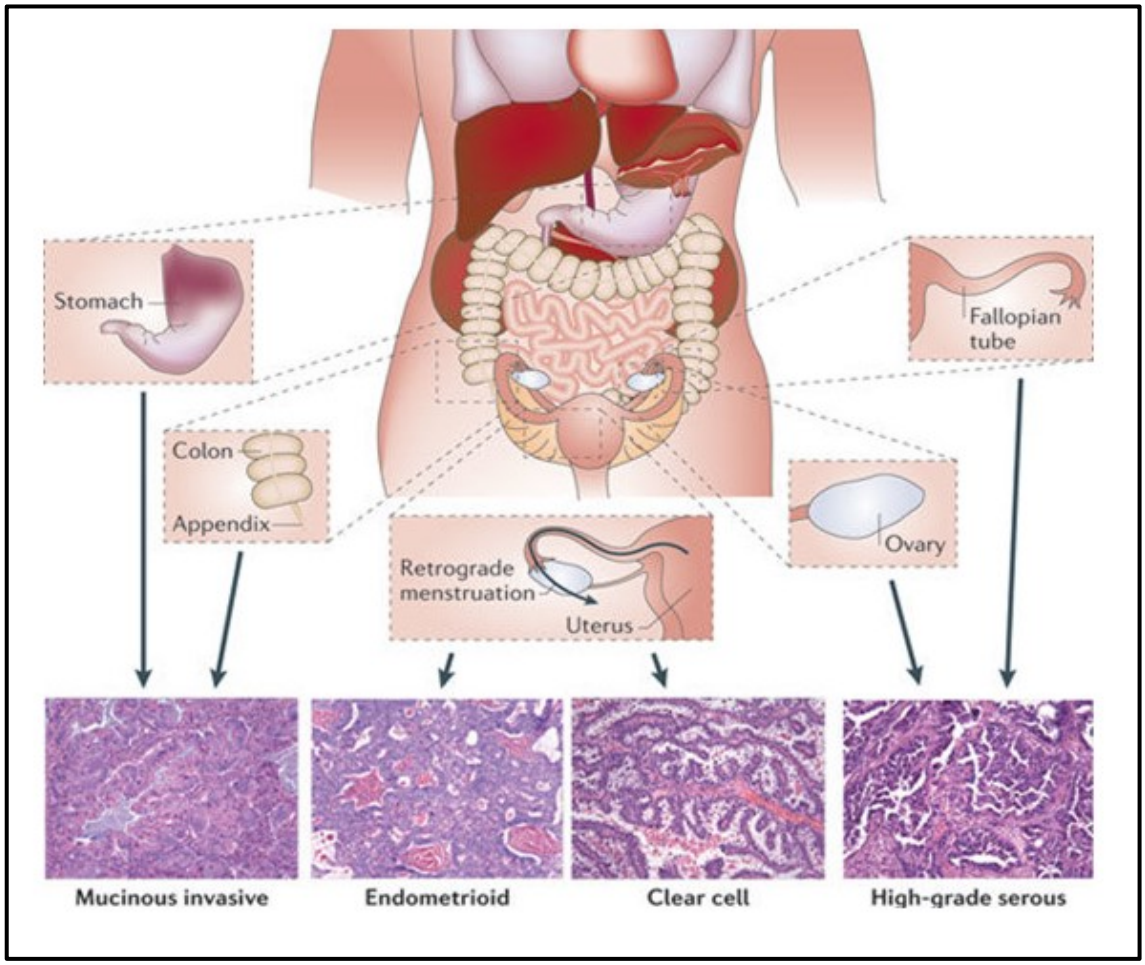

Figure 1. Epithelial ovarian cancer (EOC) histological subtypes. The upper sections display the postulated tissues of origin for the EOC histological categories. The lower sections display H&E staining of the histological subtypes. Reprinted from (6).

EOC diagnosis

The five-year survival rate for EOC is quite high, above 90%, when detected early. Unfortunately, only about 15% of EOC cases are diagnosed before the disease advances, which means the cancer is often not detected until the later stages where the five-year survival rate decreases dramatically (9). A myriad of issues can factor into limiting early detection, including nonspecific symptoms, lack of dependable biomarkers, and ineffective imaging modalities. Nonspecific symptoms include abdominal pain, swelling, or other nonspecific gastrointestinal issues. These symptoms often persist for more than 6 months prior to an EOC diagnosis (10). Upon presentation of these symptoms, a pelvic exam is often performed. However, due to the diminutive size and internal placement of the ovaries, a pelvic exam is often not sensitive enough to detect ovarian cancer (10, 11).

Other testing that is commonly performed on patients with suspected ovarian cancer includes laboratory testing such as measurement of serum carbohydrate antigen 125 (CA125) levels (10). CA125, also known as MUC16, is a heavily glycosylated transmembrane cell surface protein that is expressed by epithelial ovarian carcinomas, as well as some normal human tissues (e.g. endometrium, lung, and cornea) (12). The high molecular weight protein (5MDa) is cleaved and released into bodily fluids, such as serum. Thus, it is detectable by noninvasive procedures, such as immunoassays, and is found in 90% of patients with stage III-IV EOC and 50-60% of patients with early stage EOC (13). Because CA125 levels are not high in patients with early stage EOC and is also frequently elevated in the context of benign gynecologic conditions, such as endometriosis, uterine fibroids, pelvic inflammatory disease, and normal menstruation, it alone is not sensitive nor specific enough for early detection. Even so, CA125 is currently the most commonly used biomarker for OC. Similar results (the lack of sensitivity and specificity) have been shown with the usage of various imaging

modalities, such as transvaginal sonography (TVS), to diagnose EOC. It has recently been posited that two stage strategies, consisting of some combination of CA125 measurements and TVS, can reduce EOC mortality by providing increased sensitivity and specificity of detection (14). Another protein, human epididymal secretory protein E4 (HE4), has recently shown promise as an EOC biomarker. In normal tissue, HE4 is usually weakly expressed in the epithelium of the respiratory and reproductive tracts. However, HE4 is commonly upregulated in EOC and is similar to CA125, in that HE4 is overexpressed and secreted from ovarian carcinomas in a small glycosylated form (15). Thus, HE4 can also be detected in the serum of those with EOC. However, in contrast to CA125, HE4 has proven itself to be more specific than CA125; HE4 tends to be overexpressed in only serous and endometrioid tumors (15). The measurement of HE4 and CA125 together has been shown to be an efficient tool to diagnose OC, and may be used in conjunction with a Symptom Index or algorithms to increase the accuracy of EOC diagnosis (16, 17).

EOC stage and grade

After a diagnosis of EOC, the cancer is clinically staged. Staging is done according to the International Federation of Obstetricians and Gynecologists (FIGO), which includes Stages I-IV (7). Stage I is defined as tumors limited to the ovaries and peritoneal fluid/washings (7). Stage II is defined as metastasis from the primary tumor site to pelvic organs, as well as tumors that have extended directly to adjacent organs without evidence of formal metastasis (7). Stage III is defined as tumors that have spread from the primary site to the pelvic and abdominal peritoneal surfaces, which can involve the omentum (most common), small and large bowel surfaces, mesentery, paracolic gutters, diaphragm, and liver and spleen peritoneal surfaces (7). Stage IV is defined as distant metastasis from the primary tumor site; including parenchymal liver

and splenic metastases as well as extra-abdominal metastases (7).

In addition to the staging of ovarian cancer, the FIGO system also classifies the cancer into grades to indicate the degree of tumor cell differentiation (18). Grade 1 cancer cells are fully differentiated and similar to normal ovarian tissue, Grade 2 is moderately differentiated tumors, and Grade 3 cancer cells are either poorly differentiated or completely undifferentiated (18). In the context of serous histology OC, low-grade serous ovarian cancer is defined as grade 1, whereas high-grade serous is defined as grade 2 or 3 (19).

EOC prognosis

Poor early detection methods mean that most ovarian carcinomas are diagnosed at an advanced stage. Prognosis of ovarian cancer is strongly linked with the stage at diagnosis; the higher the stage, the poorer the prognosis (10). The grade of the cancer is also associated with prognosis, and especially with predicting disease recurrence (10). Other poor prognostic factors include: age older than 65 years, advanced stage with extensive disease, large residual tumor volume after primary surgery, clear cell or mucinous tumor histology, lower quality of life score, and poor cellular differentiation (10). Currently, inadequate early detection methods in conjunction with a lack of durable cures for advanced stage disease account for the poor prognosis of many ovarian cancer patients.

EOC treatment

The standard of care for ovarian cancer is cytoreductive surgery followed by combination chemotherapy (10). Conventional chemotherapy post-tumor debulking surgery consists of six cycles of carboplatin + paclitaxel chemotherapy (20). Paclitaxel is a taxane that works by inhibiting cell division. It does so by binding to microtubules and

stabilizing them, thus interfering with spindle formation in prophase and preventing proper mitotic progression (20). Carboplatin is a platinum agent that alkylates DNA. It creates adducts within the DNA strands, resulting in DNA crosslinking and inhibition of DNA replication and mitosis (20). The DNA damage caused by carboplatin treatment elicits a DNA damage response, and, when the damage is too great to be effectively repaired, cell death may result. The generally increased proliferative rate of cancer cells accounts for much of the anti-cancer activity of this agent.

Risk factors and protective factors for EOC

Several deleterious genetic mutations are associated with an increased risk of EOC. Most hereditary ovarian cancers are resultant from mutations within the *BRCA1* and *BRCA2* genes, which impair the homologous recombination (HR) DNA repair pathway. *BRCA1* mutation confers a mean cumulative risk for OC by age 70 of 40%, while *BRCA2* mutation confers a mean cumulative risk of 18% for OC by age 70 (21). Lynch syndrome, which is caused by mutations in the *MLH1* and *MSH2* DNA mismatch repair genes, also elevates the risk of ovarian cancer (22).

There are lifestyle factors that are non-genetic that are protective against ovarian cancer. Pregnancy, breastfeeding, and contraceptive pill usage all significantly reduce the risk of ovarian cancer (23, 24). Surgical interventions that also reduce the risk of EOC are bilateral tubal ligation and bilateral salpingo-oophorectomy (25). These surgical interventions are commonly used as prophylactic treatments in patients with high-risk of hereditary EOC.

HIGH-GRADE SEROUS OVARIAN CANCER

The cell origins of high-grade serous ovarian cancer

Since the primary site of ovarian cancer, when diagnosed, is the ovary itself, up until recently it was thought that the ovarian surface epithelium (OSE) was where the majority of the HGSC originated from. This hypothesis was also formulated was based on the incessant ovulation hypothesis, which centers around the fact that the human female ovulates monthly, and this process involves the rupturing and subsequent repair of the OSE (26). The constant damage and repair were thought to foster an environment that is primed for oncogenic transformation. Further support for this hypothesis comes from epidemiological studies that showed a relationship between the number of ovulations and the probability of a woman developing ovarian cancer, and additional factors such as multiparity and contraceptive use confer a large protective benefit, (23, 24, 25, 26).

However, more recent data suggest that the majority of HGSC may originate in the fallopian tube epithelium (FTE). The initial study that supported this idea examined fallopian tubal segments that were removed from *BRCA* mutation carriers undergoing a prophylactic bilateral salpingo-oophorectomy (24). In 12 specimens examined, six had regions of cellular dysplasia in the fallopian tubal epithelium, and five had hyperplastic lesions (27). Upon further examination, these dysplastic and hyperplastic lesions histologically resembled HGSC, without the oncogenic characteristic of invasion (27). This suggested that HGSC may originate from the FTE, rather than from the ovary itself. Additional substantiation for this hypothesis came from gene expression and DNA methylome analysis that showed that HGSC is more similar to FTE than it is to the OSE (28, 29). In the current model of the FTE origination of HGSC, p53 signatures [or early serous proliferations (ESPs)] are the earliest precursor lesions. These lesions, which are believed to emanate from secretory cells, are characterized by p53 mutations, DNA

damage, and robust nuclear localization of p53 (Figure 2) (30). Further progression leads to serous tubal intraepithelial carcinomas (STIC lesions). These lesions are identified by p53 mutations, nuclear atypia, loss of polarity, increased nuclear to cytoplasmic ratio, and high proliferative activity (31). These lesions can develop into metastatic carcinomas, developing tumors on the ovary, peritoneal cavity, or on another location on the fallopian tube (Figure 2).

Further studies utilizing mouse transgenic models also support the fallopian tube origination theory. In a mouse model where HGSC relevant genes (*BRCA1*, *BRCA2, Tp53*, and *PTEN*) were targeted to fallopian tube secretory cells, mice developed STIC lesions, HGSC, and ovarian and peritoneal metastases. These murine tumors mimicked human HGSC histologically and immunophenotypically, and displayed the genomic alterations seen in human HGSC (32). Furthermore, in another study, *Dicer*/*PTEN* dual knockout mice show high-grade serous carcinoma development in the fallopian tubes, which eventually metastasized to the ovaries and abdominal cavity. In the same study, removal of the ovaries in the mice did not prevent carcinomas from forming, whereas removal of the fallopian tubes did prevent carcinoma development (33). Finally, it should be noted that a recent mouse transgenic study demonstrates that both the OSE and the FTE can be origination points for HGSC (34). Based on the available data, it seems likely that both the FTE and the OSE play key roles in HGSC, but that OSE originated tumors are less common. Further research is needed to clarify whether FTE vs. OSE cell origin reflects two phenotypically distinct classes of HGSC.

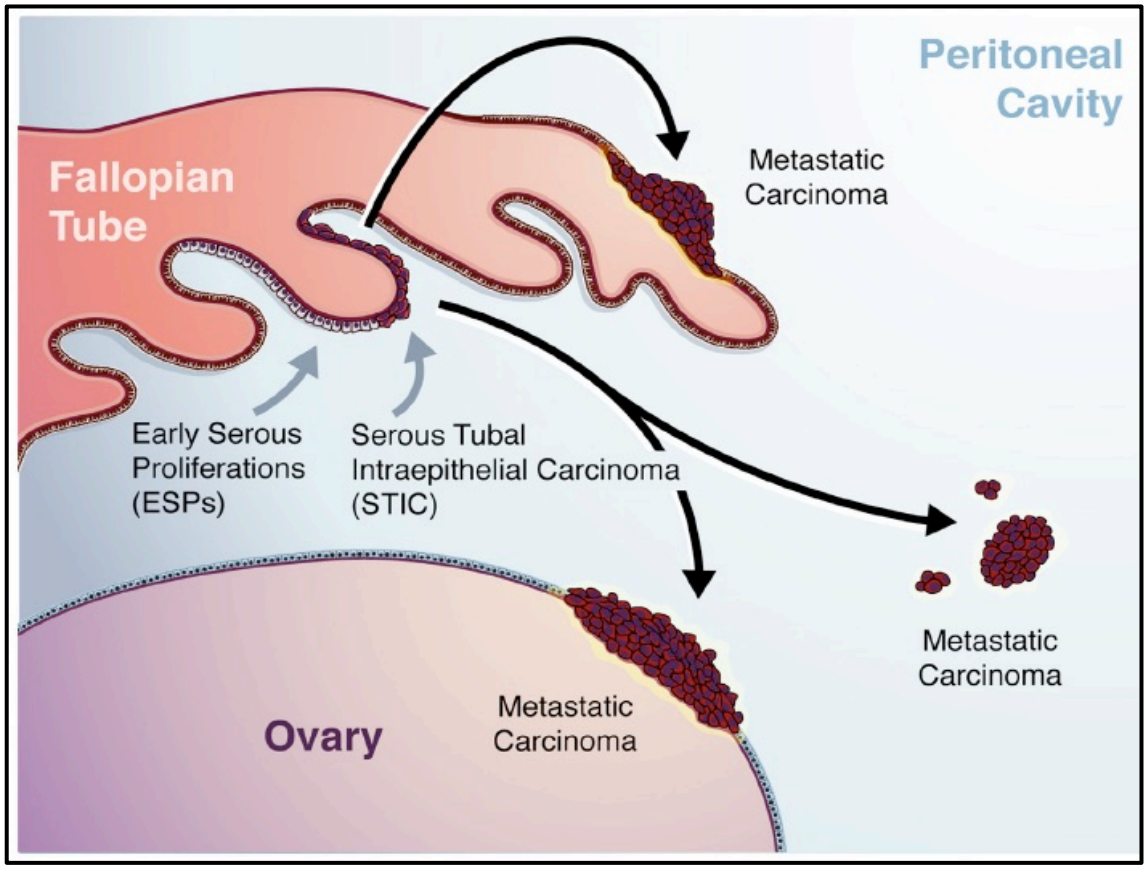

Figure 2. Model for HGSC oncogenesis from the FTE. Early serous proliferations are the earliest manifestations of HGSC oncogenesis in the fallopian tube, characterized by p53 mutations and DNA damage. The ESPs can progress into STIC lesions, which display more oncogenic characteristics such as nuclear atypia, loss of polarity, and high proliferative activity. The STIC lesions can develop into metastatic disease, moving to other sites on the fallopian tube, ovary, or peritoneal cavity. Reprinted from (31).

Genomic characteristics of HGSC

Genomic instability is a hallmark of HGSC, as shown by TCGA data, with copy number alterations (CNA) playing the major role (35, 36). One common mutation is in *TP53*. *TP53* mutations are ubiquitous in HGSC tumors and constitute the earliest observed gene abnormality in the disease, in “p53 signature lesions” (36, 37). Another important common class of mutations is in *BRCA1/2*. The mutations in *BRCA1/2* are significant because they impair the homologous recombination DNA repair (HR) in many HGSC cases, leading to the accumulation of DNA damage and genomic instability (36). However, HR impairment alone cannot account for the almost ubiquitous genomic instability observed in HGSC, as this defect is only observed in about 50% of HGSC (36). In approximately 20% of HGSC cases, *CCNE1* is amplified and is mutually exclusive with the HR deficiency caused by *BRCA1/2* mutations, thus it is a potential participant in inducing genomic instability in HGSC (38). *CCNE1* amplification and its consequent overexpression can lead to inappropriate progression through the cell cycle and induce DNA replication stress (39). Another prospective contributor to HGSC genomic instability is FOXM1. The FOXM1 pathway is activated in 84% of HGSC cases, which includes both HR proficient and HR deficient tumors (36, 40). FOXM1 is a consistent biomarker for poor prognosis in solid tumors, marking it as a possible generator of genomic instability (41, 42). In agreement, we have recently shown that FOXM1 expression in pan-cancer shows a significant association with genomic instability (43). Genomic instability is an indispensable key aspect of HGSC as it contributes to tumor evolution as well as treatment resistance. Because of this, it is imperative to determine the relevant factors driving genomic instability in HGSC (44, 45).

HGSC treatment

Treatment of HGSC follows the traditional treatment of EOC outlined above. Though there is frequently an initial positive response to platinum + taxane front-line chemotherapy in HGSC patients, around 75% of patients with advanced disease will ultimately relapse, typically within 18 months. These disease-recurrent patients are then candidates for treatment with various second-line chemotherapies (20, 46).

Importantly, HR deficiency in HGSC tumors has recently been developed as a novel treatment target. Poly ADP ribose polymerase (PARP) inhibitors have been introduced as an effective therapy for HR deficient HGSC. PARP is an enzyme involved in base excision repair (BER) of DNA (47). The PARP inhibitors work by blocking the release of the PARP molecule from the DNA strand, inhibiting BER. Later collision of PARP protein adducts with the DNA replication machinery leads to double strand breaks, which requires HR for error-free repair. Thus, this makes PARP inhibitors an attractive therapy for treating *BRCA1/2* mutated HGSC, as HR is compromised in these tumors. HR deficiency leads to reliance on other more deleterious DNA repair pathways, such as nonhomologous end-joining (NHEJ), causing an accumulation of DNA damage and subsequent cell death (47). This is known as synthetic lethality, which occurs between two genes when a mutation/loss of either gene alone retains a viable phenotype, but a mutation/loss of both genes leads to cell death (48). In this case, HR deficiency (e.g. due to BRCA mutation) is synthetically lethal with PARPi treatment. Clinical trials have shown selective toxicity of the PARP inhibitors towards *BRCA1/2* mutated tumors (49, 50, 51). Consequently, the PARP inhibitor olaparib was FDA approved for treatment of *BRCA*-mutated ovarian cancers in 2014 (52, 53). It has been found, however, that not all patients that are treated with PARP inhibitors respond, and those that do respond typically develop resistance (54, 55, 56, 57). This shows that investigating methods to overcome PARP inhibitor resistance in *BRCA* mutant HGSC,

and identifying means to better target HR competent tumors with PARPi, is of great importance.

FOXM1

FOXM1 structure, expression, and regulation

The discovery of FOXM1 occurred during a cDNA screen, where it was initially dubbed M-phase phosphoprotein 2 (MPP-2), as it was identified as a protein phosphorylated during the M phase of the cell cycle (58). Other original terms used to refer to FOXM1 include Trident (murine), WIN or INS-1 (rat), MPP-2 (human c-DNA), and HFH-11. Further research into FOXM1 determined that it had similar molecular features to the Forkhead box (FOX) family of transcription factors. The FOX transcription factor family, which has approximately 50 members in humans, is unified by a conserved winged helix DNA binding domain, and FOXM1 shares a sequence motif in this region with other members of the FOX family (59, 60).

FOXM1 is characterized by a DNA binding domain, a transactivation domain (TAD) (located at the C terminus), and an N terminal repressor domain (NRD). The TAD is crucial for activating expression of target genes and the NRD can repress the TAD by interacting directly with it (61, 62). The human locus of *FOXM1* is on chromosome 12p13.33 and includes 10 exons (9 are coding), with alternative splicing giving rise to four different FOXM1 isoforms: *FOXM1a*, *FOXM1b*, *FOXM1c*, and *FOXM1d*. These splice variants are achieved by alternative splicing of exons Va and VIIa. FOXM1a contains both exons Va and VIIA, FOXM1b contains neither exon, FOXM1c contains Va, and FOXM1d contains VIIa (Figure 3). FOXM1a appears to be transcriptionally inactive, whereas FOXM1b, FOXM1c, and FOXM1d act as transcriptional activators (43, 58, 63). It was previously thought that FOXM1a was inactive due to the presence of VIIa in the transactivation domain, however FOXM1d also contains VIIa and has been identified as

promoting the epithelial-mesenchymal transition by activating a protein called ROCKS in colorectal cancer (63). In normal tissues, HGSC cell lines, and pan-cancer, *FOXM1c* is the most highly expressed FOXM1 isoform, while *FOXM1b* shows moderate expression and *FOXM1a* shows the lowest expression (40, 43).

FOXM1 mRNA and protein are expressed in a cell cycle dependent manner, upregulated during S phase and expression peaking at the G2/M boundary (58). Similarly, FOXM1 activity follows a cell cycle dependent pattern. FOXM1 activation is mediated primarily through phosphorylation by various kinases, and the transcriptional activity of FOXM1 is influenced by its phosphorylation state. Phosphorylation of FOXM1, and thus activation of FOXM1, begins in late G1 and sequential phosphorylations occur as the cell cycle progresses, generating the hyperphosphorylated and fully active form of FOXM1 by the G2/M boundary (62). One phosphorylation reaction of note is the phosphorylation of FOXM1 at residues S331 and S704 by the Raf/MEK/MAPK pathway, upon which FOXM1 is subsequently shuttled from the cytoplasm into the nucleus, where further phosphorylation and activation can occur (62, 64).

FOXM1c is the most highly expressed FOXM1 isoform in HGSC and has its own unique pattern of phosphorylation sites. It contains the residues needed for the above phosphorylation by the Raf/MEK/MAPK pathway, as well as CDK1/2 phosphorylation sites (Figure 4). In conjunction with a partner cyclin (cyclin A or cyclin E1), CDK1/2 phosphorylate FOXM1c at residues 600, 611, and 672 during G2 phase, which relieves repression of the TAD by the NRD (64, 65, 66).

Additional regulation of FOXM1 is achieved through micro RNAs (miRNAs). Many studies have been done on various miRNAs with the capability to modulate FOXM1 expression. miRNA are small, non-coding RNA molecules that can bind to target mRNAs via complementary base-pairing. This prevents translation of the mRNA by various means: destabilization of the mRNA, cleavage of the mRNA, or the inability to be

translated by the ribosome due to being bound by the miRNA. One miRNA that has been studied extensively in regard to FOXM1 regulation is miRNA-149. By targeting and binding to *FOXM1*, miRNA-149 has been shown to inhibit growth, migration, and invasion of colorectal cancer cells and to reverse resistance to 5-fluorouracil, a chemotherapy agent (67, 68). In another type of cancer, non-small-cell lung cancer, miRNA-149 was shown to prevent the epithelial-to-mesenchymal transition promoted by FOXM1 (69).

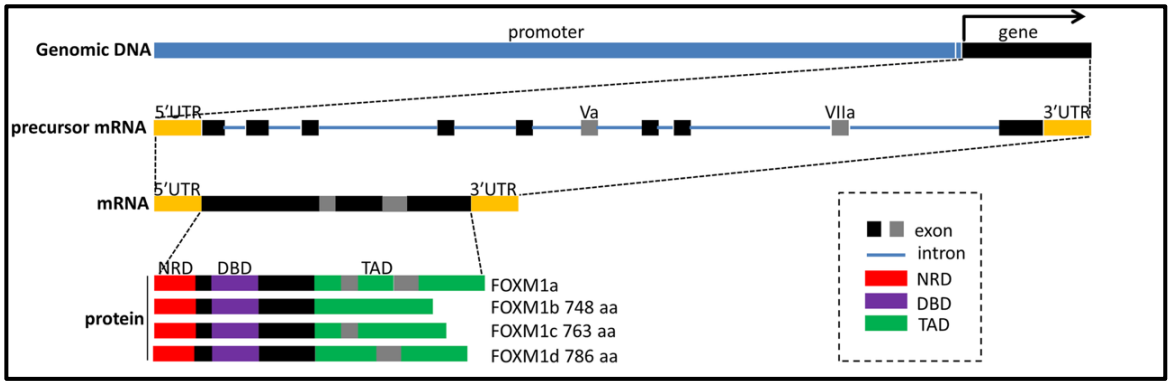

Figure 3. Genomic structure and isoforms of FOXM1. The gene region of *FOXM1* is transcribed into precursor mRNA. The precursor mRNA has a 5' untranslated region (UTR) and a 3' UTR, with 9 introns and 10 exons. Va and VIIa are two alternative exons. The mRNA undergoes alternative splicing to remove the introns and give rise to the different isoforms of *FOXM1*. All splice variants contain a nuclear repression domain (NRD), DNA binding domain (DBD), and transactivation domain (TAD). FOXM1a contains both exons Va and VIIA, FOXM1b contains neither exon, FOXM1c contains Va, and FOXM1d contains VIIa. Reprinted from (62, used under a Creative Commons Attribution 4.0 International license: https://creativecommons.org/licenses/by/4.0/legalcode)

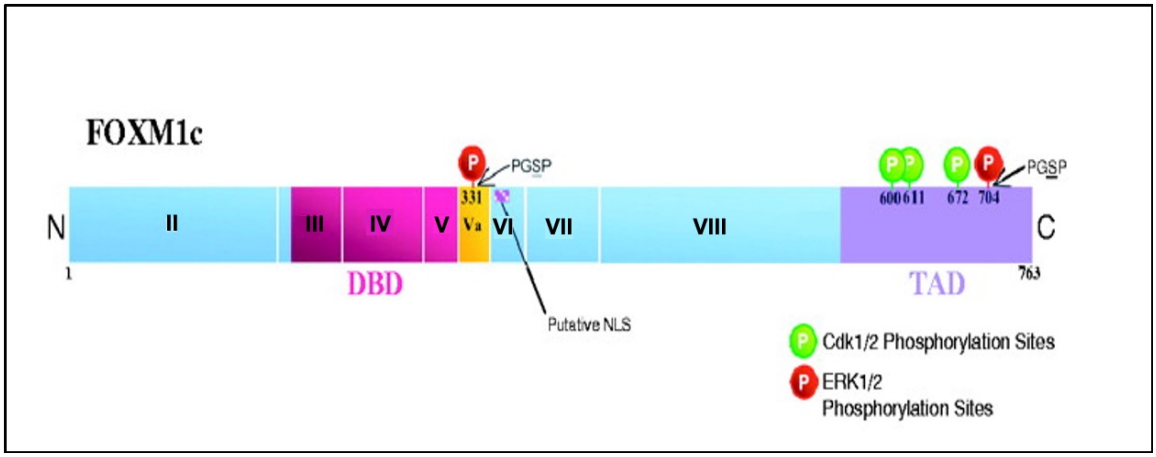

Figure 4. FOXM1c protein diagram. FOXM1c is comprised of eight exons, denoted by the roman numerals (II-VIII); in contrast to other isoforms, it contains only alternative exon Va. The N terminus is followed by a DNA binding domain (DBD). The transactivation domain (TAD) is near the C terminus. ERK1/2 phosphorylates FOXM1c at residues 331 and 704, and CDK 1 and 2 phosphorylate FOXM1c at residues 600, 611, and 672. Reprinted from (64).

FOXM1 function

FOXM1 is a transcription factor crucial for cell cycle progression, particularly through the G1/S and G2/M checkpoints, and for mitotic progression (70). Exemplifying this, studies showed FOXM1 knockout MEFs proliferated slowly, did not enter mitosis correctly, accumulated mitotic defects, and eventually went into cellular senescence (71, 72). More in depth examination into the mechanisms that FOXM1 may be involved with revealed that FOXM1 is important for appropriate chromosomal segregation, as loss of FOXM1 caused genomic instability including the accumulation of polyploid cells (73, 74). Furthermore, the transcriptional targets of FOXM1 are involved with mitotic progression, proper assembly of mitotic spindles, proper chromosome segregation, and cytokinesis (75, 76). In summary, cell cycle regulation is the canonical function regulated by FOXM1 transcriptional activity (59, 77). Additionally, FOXM1 has a role in DNA repair, cell migration, stemness, and chemoresistance (78, 79, 80). FOXM1 does this by upregulating the expression of genes involved in these processes.

FOXM1 and cancer

FOXM1 is both overexpressed and functionally activated in many human cancers and has been found to have oncogenic activity both *in vitro* and *in vivo* (77, 43). The processes underlying FOXM1 overexpression in cancer are many and include genomic amplification (40, 43), p53 mutation (81, 82), Rb loss of function (40), FOXO3 loss (83, 84), and Myc, HIF-1, SP1, STAT3, Gli1, and E2F activation (85, 86, 87, 88, 89, 90).

FOXM1 activation is achieved through phosphorylation by mitogenic kinases and cyclin/CDK complexes, which are frequently dysregulated in cancer. Through its role as a transcription factor, FOXM1 stimulates oncogenic phenotypes and induces progression through the G2/M checkpoint (77). Overexpression and improper activation

of FOXM1 can contribute to an oncogenic phenotype by spurring cells through the cell cycle inappropriately, leading to increased cellular proliferation.

Two of the hallmarks of cancer are deregulation of the cell cycle and uncontrolled cellular proliferation; deregulation of the cell cycle and subsequent uncontrolled proliferation are the most common oncogenic phenotypes associated with FOXM1. In both spontaneous and genetically engineered animal models of cancer, ectopic expression of FOXM1 leads to larger tumors and quicker tumor formation (91).

Beyond cell cycle regulation, additional oncogenic roles that FOXM1 is associated with include cancer cell stemness, chemoresistance, genomic instability, and DNA replication stress (80, 91, 92). Of particular note, a study showed that downregulation of FOXM1 reduced the expression of invasion related proteins matrix metalloproteinase-2, matrix metalloproteinase-9, and vascular endothelial growth factor, which are proteins involved in invasion and angiogenesis. This downregulation of FOXM1 also inhibited cell growth and decreased both migration and invasion of pancreatic cancer cells (79).

CCNE1

CCNE1 structure, expression, and regulation

CCNE1 was discovered in 1991, via a screen of human cDNAs that compensated for the loss of yeast interphase cyclins (93). Cyclins are a class of proteins that each have its own unique protein/expression degradation profiles that correspond to specific phases of the cell cycle. Functionally, cyclins bind to cyclin dependent kinases (CDKs) to phosphorylate and coordinate specific events related to the cell cycle position (94). *CCNE1* is located on chromosome 19.q12 and is 12,415 base pairs long (95). There are nine protein splice variants, with CCNE1-like isoform 1 (E1L) considered the canonical major form that complexes with CDKs (96). The major form, E1L, is comprised

of 410 amino acids and has two domains made up of five alpha helices each (97) (Figure 5). The protein contains both a nuclear and centrosome localization sequence, along with a conserved cyclin box (98).

The protein expression of CCNE1 increases through G1, peaks at the G1/S boundary, and is degraded in S phase (99). In the cell, it is located in both the cytoplasm and the nucleus, though it is primarily nuclear (100). Transcriptional regulation of *CCNE1* occurs through phosphorylation of the Rb/E2F complex by the cyclin D (CCND) and CDK4/6 complex. Rb phosphorylation leads to the dissociation of E2F1-3 from Rb and allows E2F to bind to E2F binding sites within the *CCNE1* promoter, promoting transcription of *CCNE1*. The newly made CCNE1 protein then continues to promote the phosphorylation of the Rb/E2F complex, allowing further activation of E2F and upregulation of CCNE1 in a positive feedback loop (101). Another common mechanism of CCNE1 transcriptional regulation is through C-Myc, which upregulates CCND1, causing increased phosphorylation of the Rb/E2F complex and E2F activation (102). In contrast, negative regulation of *CCNE1* is achieved through repression by E2F4-6, which recruit factors such as histone deacetylases, methylation complexes SUV39H1 and HP1, and nucleosome remodeling complexes to decrease *CCNE1* transcription during S phase, after CCNE1's function to activate proteins involved in the progression through the G1/S boundary has been completed (98).

CCNE1 is also regulated post-transcriptionally through microRNA mediated inhibition of CCNE1 synthesis, inhibition by p21 and p27 (which block CDK binding to the cyclin subunit), and through ubiquitin mediated degradation (through both the Cul3 and SCF^{Fbw7} pathways) (98).

CCNE1 function

Cyclins bind with a CDK subunit, upon which a conformational change in the

CDK occurs that opens up the active site and the ATP binding pocket. Both inhibitory and activating phosphates are modulated; the complex is not able to fulfill its activity until the inhibitory phosphate has been removed by a phosphatase.

CDK2 is the major CDK binding partner of CCNE1, as it binds with the highest affinity. CCNE1 binds to CDK2 primarily through the C-(PSTAIR) helix and the activation segment of CDK2 (97) (Figure 5). The activation segment of CDK2 is crucial for protein substrate recognition (97). CCNE1 can also bind CDK1 and CDK3, with CDK1 able to promote the G1/S transition in CDK2 null MEFs (103).

CCNE1 has a myriad of functions, some CDK dependent and some CDK independent. A major CDK dependent function of CCNE1 is mediating G1/S transition. One of the major ways this is accomplished is through phosphorylation of Rb by the CCNE1/CDK complex. The complex phosphorylates Rb, releasing E2F proteins and promoting transcription of critical genes that promote S phase initiation and progression (98).

Some of the other CDK2 dependent functions of CCNE1 are centrosome duplication, histone gene transcription, DNA synthesis, and DNA repair (98). The CDK independent functions of CCNE1 involves also centrosome duplication as well as pre-initiation complex formation (98). For the latter, CCNE1 is loaded onto chromatin during the G0 into S phase progression and facilitates the minichromosome maintenance complex component 2 (MCM2) loading onto chromatin through interactions with the MCM2 and chromatin licensing and DNA replication factor 1 (CDT1). These activities help promote pre-initiation complex formation prior to centrosome duplication (98, 104).

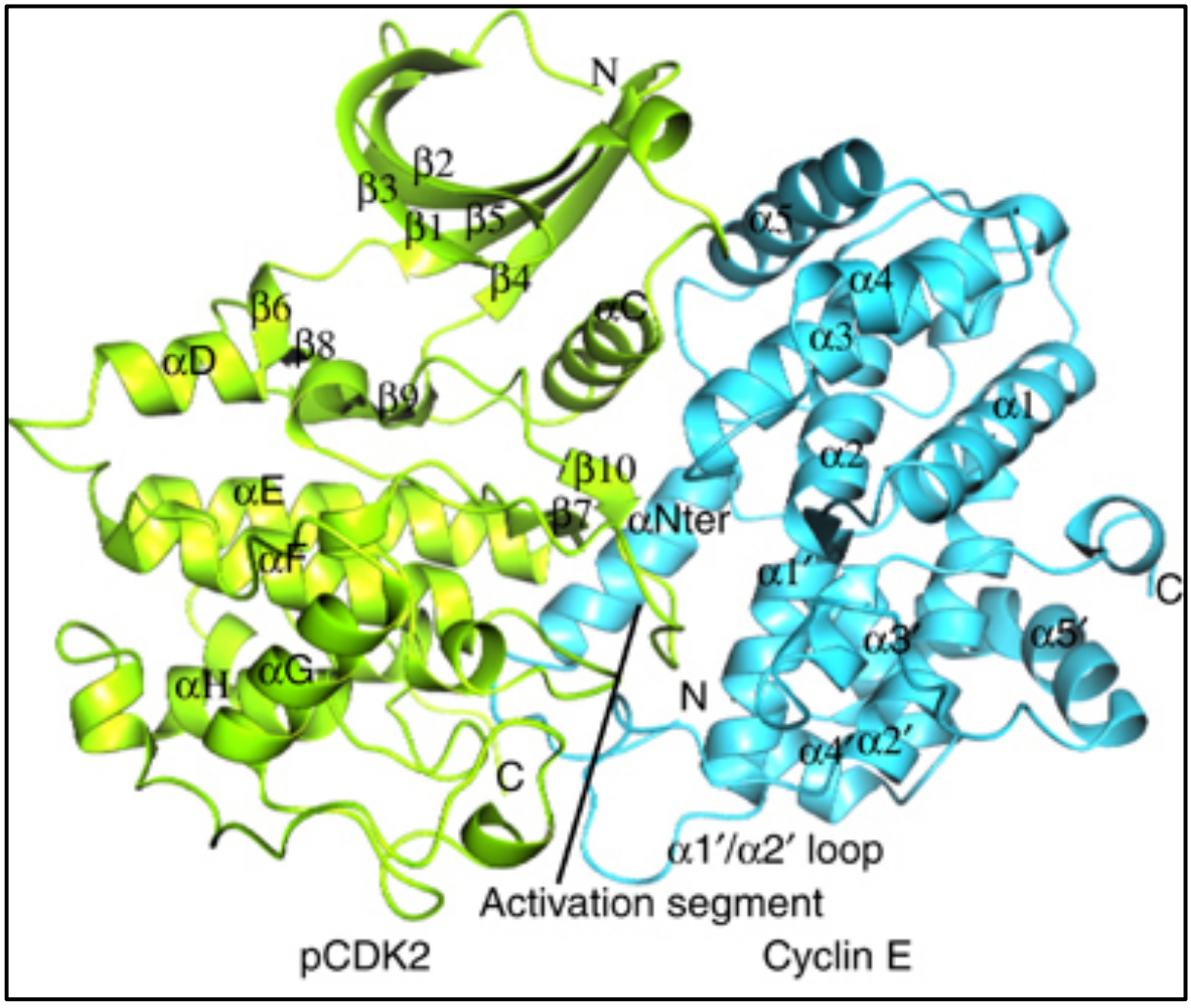

Figure 5. Crystal structure of CCNE1 complexed with p-CDK2. CCNE1 is comprised of two domains made up of five alpha helices each. CDK2 contains both alpha helices and beta sheets. The activation segment of CDK2 is crucial for protein substrate recognition. Reprinted from (97).

CCNE1 and cancer

CCNE1 is frequently overexpressed in cancer, and one mechanism of this is through *CCNE1* gene amplification. For example, *CCNE1* is amplified in 20% of HGSC cases (36). However, increased expression of CCNE1 in HGSC is not only due to genomic amplification, as the number of CCNE1 overexpressing HGSC cases is twice as high as *CCNE1* amplified cases, suggesting other methods of CCNE1 overexpression (105).

A potential contributor to oncogenesis may be the increased expression of low molecular weight (LMW) cyclin E1 protein isoforms. CCNE1 exists in nine isoforms, however five of these are seen only in cancer (106). The cyclin E-like isoforms (EL), EL-2, 3, 5, and 6, are generated by proteolysis at two proteolytic sensitive domains in CCNE1, and the fifth isoform originates from an alternative translation site. All of these isoforms are low molecular weight, ranging from 34-49 kDa, whereas the EL-1, the canonical major form, is ~50 kDa (Figure 7) (96). These LMW forms have a higher affinity for CDK2 , thus they are more biologically active and phosphorylate substrates more readily (96,105).

Other mechanisms leading to the increased expression of CCNE1 observed in cancer is homozygous deletion of Rb (leading to constitutive activity of E2F and subsequent transcription of *CCNE1*), *MYC* amplification (also leading to increased transcription of *CCNE1*), or a mutation in SCF^{Fbw7} (leading to decreased degradation of cyclin E1through a ubiquitin mediated pathway) (105).

The results of cyclin E1 overexpression in cancer are improper DNA replication initiation, replication stress, and inappropriate centrosome duplication, ultimately leading to the accumulation of mutations that promote oncogenesis (107, 108).

CCNE1 and HGSC

Analysis of TCGA data for 22 different cancer types revealed that *CCNE1* is commonly amplified in gynecological cancers, gastrointestinal cancers, and lung cancers (38). Importantly, *CCNE1* was the most commonly amplified gene in HGSC (38). Cyclin E1 expression is associated with the beginning stages of HGSC development; STIC lesions have increased *CCNE1* copy number gain/amplification and have increased expression of cyclin E1 by IHC (Figure 6). Ectopic expression of CCNE1 in FTE cells, the presumed HGSC precursor cells, promoted hallmarks of transformation, including cell proliferation, anchorage independent growth, and loss of contact inhibition (39).

Knockdown of CCNE1 in *CCNE1* amplified ovarian cancer cells led to significant growth inhibition and increased apoptosis, in comparison to cancer types that had low CCNE1 levels, and ectopic expression of cyclin E1 increased proliferation in the cancer cell lines with low basal cyclin E1 expression (109). These data support that cyclin E1 plays a crucial role in mediating oncogenic HGSC phenotypes.

As noted before, germline *BRCA1/2* mutations are the predominant genetic risk factor for HGSC, and so a closer look into the role that CCNE1 and BRCA1/2 disruptions may play together in HGSC oncogenesis is needed. Using data from a genome-wide shRNA synthetic lethal screen, a study showed that BRCA1 and members of the ubiquitin pathway are selectively required in cancers that harbor CCNE1 amplification. As such, *CCNE1* amplification was found to be mutually exclusive with *BRCA1/2* mutations (38). Mechanistically, *CCNE1* amplified tumors have increased DNA damage, which requires an effective homologous recombination repair pathway for resolution. Therefore, *BRCA1/2* mutations and CCNE1 amplifications are not harbored together in HGSC as it would be synthetically lethal. Interestingly, this may mean that one of the typical chemotherapies used in HGSC treatment, carboplatin, may not be as effective in tumors

with *CCNE1* amplifications, as such tumors are not HR deficient and thus can effectively repair double strand DNA breaks caused by drug treatment (38).

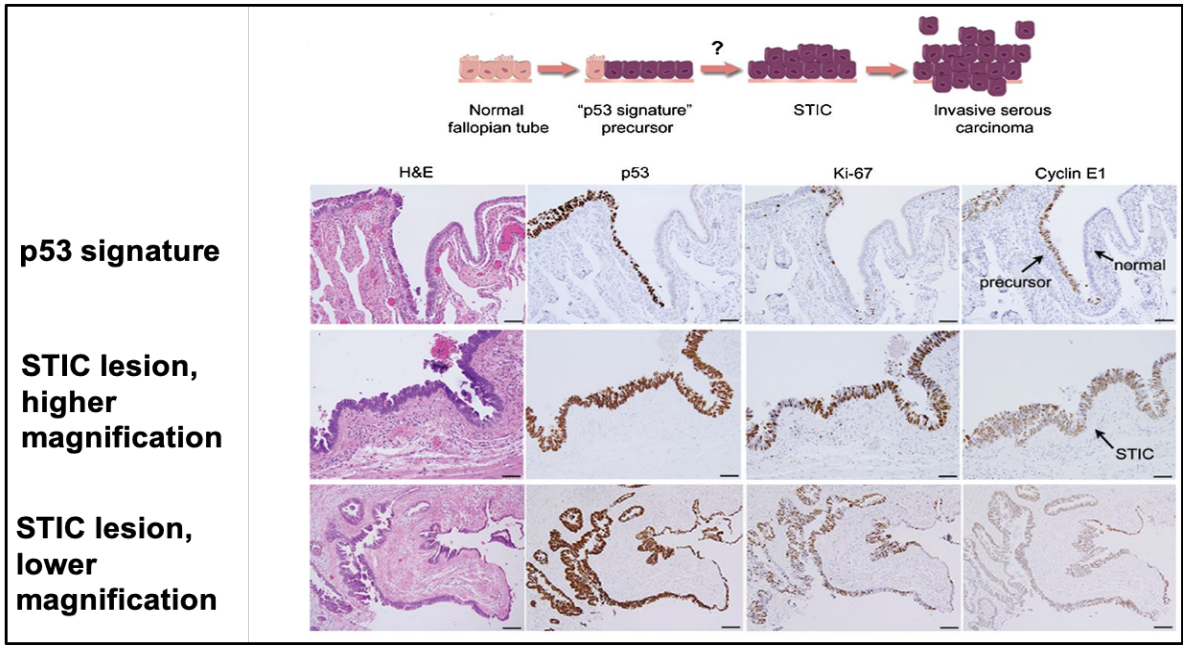

Figure 6. Cyclin E1 expression in HGSC precursor lesions. A cartoon illustrating the progression of HGSC from normal FTE is shown at the top. p53 signatures arise first, followed by the development of STIC lesions. These lesions progress even further into invasive serous carcinomas. The lower portion of the figure shows H&E and IHC staining of a p53 signature and a STIC lesion. The top row shows the staining of the p53 signature, with high level staining of mutant p53 and lower levels of Ki-67 and Cyclin E1 staining. The lower two rows represent a STIC lesion, showing staining for mutant p53, Ki-67, and CCNE1. Reprinted from (39).

The potential for FOXM1 and CCNE1 cooperativity in HGSC

FOXM1 and CCNE1 each contribute to HGSC as well as other cancers. Since FOXM1 contains residues that are known to be phosphorylated by CDK complexes, it may be that the CCNE1/CDK complex has a role in a phosphorylation event that activates FOXM1. A study published in 2006 provided evidence for a CCNE1/CDK2 interaction with FOXM1, showing that CCNE1/CDK2 enhanced FOXM1 transcription in a reporter gene assay, and that three amino acid residues within the FOXM1 protein are CCNE1/CDK2 phosphorylation sites (65). Also of note, our prior analysis of TCGA data indicates that FOXM1 and CCNE1 mRNA and protein expressions are strongly correlated (43). Moreover, we have shown that ectopic expression of CCNE1 increases FOXM1 expression in FTE cells (43). CCNE1 enhances FOXM1 transcriptional activity and CCNE1/FOXM1 co-expression also promotes genomic instability (92, 43). All of these data suggest that CCNE1 and FOXM1 may cooperate in HGSC, potentially in part through activation of FOXM1 by phosphorylation by CCNE1/CDK complexes. To address these important questions, we wanted to determine the impact that the CCNE1/CDK complexes have on FOXM1 phosphorylation status in FTE cells and HGSC, as well as investigate the effect that CCNE1 and FOXM1 together have on FTE cellular transformation phenotypes.

CHAPTER 2: MATERIALS AND METHODS

Human tissues

Bulk normal ovary (NO) tissues and EOC samples (n=42) were obtained from patients undergoing surgical resection at Roswell Park Comprehensive Cancer Center (RPCCC) under Institutional Review Board-approved protocols, as described previously (119). Flash-frozen bulk tumor tissue samples were crushed using liquid nitrogen pre-chilled mortar and pestles. Total protein was extracted using radioimmunoprecipitation assay (RIPA) buffer (25 mM Tris HCl pH 7.6, 150 mM NaCl, 1% NP-40, 1% sodium deoxycholate, 0.1% sodium dodecyl sulfate (SDS)) containing Protease Inhibitor Cocktail (SIGMA), Phosphatase Inhibitor Cocktail 1 (SIGMA) and Phosphatase Inhibitor Cocktail 2 (SIGMA). Upon the addition of RIPA buffer, the frozen tissue powder was immediately homogenized using an electric homogenizer with disposable microtube pestles. The solution was further sonicated with a Bioruptor (Diagenode).

Cell lines

COV362 and COV318 cell lines (Sigma) were cultured in DMEM (Corning) supplemented with 10% fetal bovine serum (FBS, Invitrogen), 2 mM glutamine (Life Technologies), 1% penicillin-streptomycin (pen-strep, Life Technologies). KURAMOCHI and OVSAHO (Japanese Collection of Research Bioresources Cell Bank) and SNU-119 (Korean Cell Line Bank) cell lines were cultured in RPMI-1640 (Hyclone) supplemented with 10% FBS and 1% pen-strep. OVCAR3 cells (American Type Tissue Culture Collection) were cultured in DMEM with 10% FBS and 1% pen-strep. Caov3 and OVCAR5 cells were a generous gift from Professor Anirban Mitra (Indiana University) and were cultured in DMEM with 10% FBS and 1% pen-strep. OVCAR8 cells (National Cancer

Institute Division of Cancer Treatment and Diagnosis Cell Line Repository) were cultured in DMEM (Corning) supplemented with 10% FBS and 1% pen-strep, Life Technologies. Fallopian tube epithelial (FTE) cells immortalized with hTERT and mutant Tp53 (FT282 cells) were a generous gift from Professor Ronny Drapkin (University of Pennsylvania) and were cultured in DMEM-Ham's F12 50/50 (Corning) supplemented with 10% FBS and 1% pen-strep (Figure 7). Clonal FT282 cells (FT282-C11) cells were generated as described previously (112). All cell lines were maintained at 37°C in a humidified incubator with 5% CO2. Cell culture medium was changed every 3-5 days depending on cell density. For routine passage, cells were split at a ratio of 1:4-10 when they reached 85% to 90% confluence. Cell lines were authenticated by short tandem repeat (STR) analysis at the DNA Services Facility, University of Illinois at Chicago, and tested for mycoplasma, and confirmed to be mycoplasma free, by RT-qPCR at the Epigenomics Core Facility, University of Nebraska Medical Center.

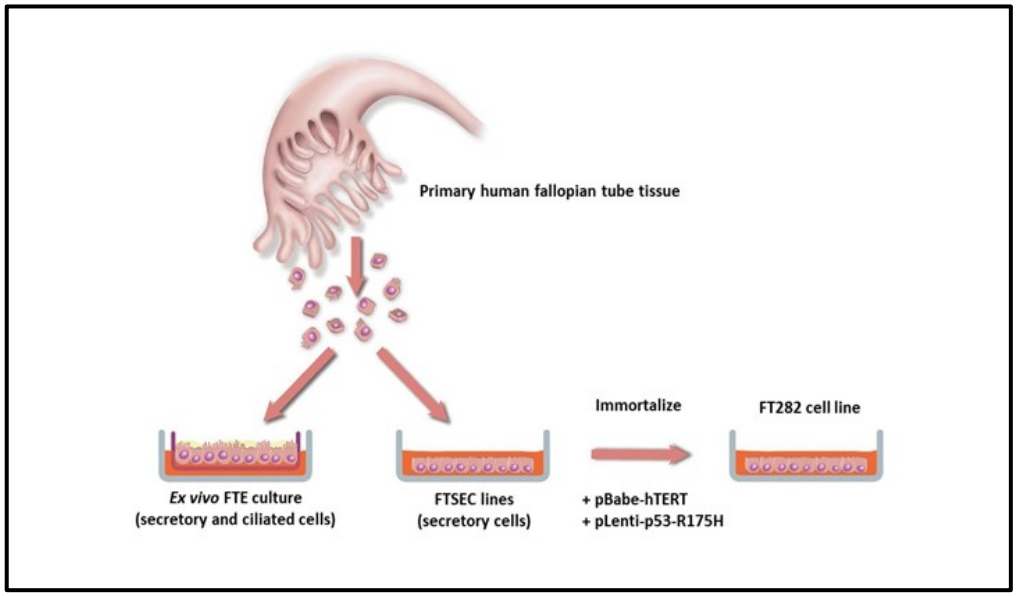

Figure 7. Generation of an immortalized fallopian tube epithelial cell line (FT282). FTE cells were removed from the lining of the fallopian tube. Fallopian tube secretory cells (FTSEC) are able to grow on plastic whereas ciliated cells cannot. FTSEC were immortalized by transduction with lentivirus expressing mutant p53 and retrovirus expressing h-TERT. Cells surviving antibiotic selection are immortalized but non-transformed. Reprinted from (111).

Generation of FT282-CCNE1, FT282-FOXM1c, and FT282-CCNE1 + FOXM1c ectopic expression cell lines

pCW57-MCS1-2A-MCS2 (Addgene #71782) was generated by converting pCW57.1 (Addgene #41393) from Gateway cloning to sticky end cloning by adding a multiple cloning site. pCW57-CCNE1 (RefSeq NM_001322262) was generated by PCR subcloning *CCNE1* (Harvard PlasmID Repository, HSCD00326535, RefSeq NM_001322261) into pCW57-MCS1-2A-MCS2. The tetracycline-inducible lentiviral pCW57.1-DDK-FOXM1c vector was generated by subcloning human *FOXM1c* from pCMV6 (Origene: SC112825) into –AN-DDK plasmids (Origene: PS100014), then subcloning into the pCW57.1 (Addgene: 41393) with Gateway cloning (Life Technologies).

Replication-deficient lentivirus was produced by transient transfection of 6.0 µg psPAX2 (Addgene #12260), 2.0 µg pMD2.G (Addgene #12259), and 8.0 µg transfer plasmid into HEK293T (293T) cells in a 10 cm dish with Lipofectamine 2000 reagent (Life Technologies, Carlsbad, CA, USA), according to the manufacturer's instructions. Viral supernatants were collected at 48 h and passed through a 0.2 µm filter. Functional titration was performed by transduction of 293T cells with serially diluted virus in the presence of polybrene (4 µg/mL, Sigma) for 6 h followed by puromycin (Life Technologies) selection 48 h post-infection. After selection, cells were allowed to recover and were expanded.

Cell line	Vector	Vector type	Expression	Protein overexpressed
FT282	pCW57	Lentiviral	Dox inducible	None; empty vector
FT282 FOXM1c	pCW57	Lentiviral	Dox inducible	FOXM1c
FT282 CCNE1	pCW57	Lentiviral	Dox inducible	CCNE1
FT282 CCNE1/FOXM1c	pCW57	Lentiviral	Dox inducible	CCNE1 and FOXM1c

Table 1. FTE cell lines used in this study. Note: all FT282 cells lines are from clonal derivative (FT282-C11) reported previously (112).

Pharmacological Inhibitors and cellular treatments

Cells were treated with CDK inhibitors (CDKi) dinaciclib (ab219469, solubilized in DMSO) from Abcam, R03306 (solubilized in DMSO), palbociclib (solubilized in DMSO), AT7519 (solubilized in DMSO) from Selleck. 1 µg/mL of doxycycline (dox) was added to the media of FT282 cell lines 24 hours post seeding, and CDKi was added 24 hours post-dox treatment. 24 hours after the addition of CDKi, cells were harvested and total cellular proteins were extracted. In other experiments, OVCAR8 cells were treated with CDKi 24 hours post-seeding and, 24 hours later, nuclear and cytoplasmic proteins were extracted.

Protein extractions and Western blot analyses

Whole cell protein extracts were prepared using RIPA buffer [1X PBS, 1% NP40, 0.5% sodium deoxycholate, 0.1% SDS] supplemented with protease and phosphatase inhibitors (Sigma). RIPA extracts were centrifuged at 4°C for 10 minutes at 14000g, and the supernatant fraction was harvested. Nuclear extracts were prepared using the NE-PER Nuclear and Cytoplasmic Extraction Kit (Thermo Scientific) supplemented with protease and phosphatase inhibitors. Protein concentrations were determined using BCA protein assays (Thermo Scientific). Equal amounts of protein (20-50 µg) were fractionated on 4-12% gradient SDS-polyacrylamide gel electrophoresis gels (Invitrogen) and transferred to PVDF membranes (Roche). Membranes were stained with Ponceau S to confirm efficient transfer and equal loading, and binding of non-specific proteins were blocked using 5% nonfat dry milk in Tris-buffered saline Tween-20 (TBST) for 1 hour at room temperature. The membranes were then incubated with primary antibody in 5% nonfat dry milk in TBST at 4°C overnight followed by incubation with secondary antibody in 5% nonfat dry milk in TBST for 1 hour at room temperature. Primary and secondary antibodies information are provided in Table 3. Enhanced chemiluminescence (Pierce

ECL Western Blotting Substrate, Thermo Fisher Scientific, catalog no. 32106 and Supersignal West Pico Plus Chemiluminescent Substrate, Thermo Fisher Scientific, catalog no. 34580) were used for protein detection, in conjunction with photographic film developing. Quantification of protein bands on film images were performed using ImageJ software (Image Processing and Analysis in Java, National Institute of Health).

Antibody	Company	Catalog Number	Application	Dilution
p-FOXM1 (T600)	Cell Signaling	14655S	Western Blot	1:1000
FOXM1	Cell Signaling	5436	Western Blot	1:1000
CCNE1	Santa Cruz	sc-247	Western Blot	1:1000-1:10000
beta-Actin	Santa Cruz	sc-47778	Western Blot	1:5000-1:10000
CDK2	Santa Cruz	sc-6248	Western Blot	1:500
CDK1	Cell Signaling	91165	Western Blot	1:1000
Anti-mouse IgG, HRP-linked antibody	Cell Signaling	7076S	Western Blot	1:1000-1:10,000
Anti-rabbit IgG, HRP-linked antibody	Cell Signaling	7074S	Western Blot	1:500-1:10,000

Table 2. Primary and secondary antibodies used in this study.

In vitro clonogenic survival assays

To assess clonogenic survival (a.k.a. colony formation), cells were trypsinized, counted, and seeded at a density of 500 cells per well in 6-well tissue culture plates. 1 µg/mL dox was added directly to the media 24 hours after seeding and replenished every 48 hours. The plates were incubated for 8 days. Following incubation, cells were fixed using ice cold 100% methanol, rinsed with PBS, and stained with 0.5% crystal violet for 30 minutes at room temperature. After staining, the cells were rinsed with Millipore filtered water and air dried overnight. Colonies containing over 50 cells were counted using Image J software.

Direct cell counting assays

Cells were seeded at a density of 20,000 cells per well into six-well plates, seeding each cell line in triplicate. A separate plate was seeded for each day of counting. 24 hours post seeding, medium was replaced with fresh medium containing 1 µg/mL dox and dox was replenished every 48 hours throughout the experiment. Beginning at 24 hours after the addition of dox, cells were counted. To count cells, wells were washed with room temperature PBS, trypsinized, centrifuged at 500g for five minutes, resuspended in one mL of media, and counted using a Bio Rad automated cell counter, model number TC20. Cell counting was repeated every 24 hours for 5 days and the experiment was repeated three times.

Cell invasion and migration assays

Assays were performed using Corning Biocoat Matrigel Invasion Chambers (control plates catalog no. 354578; invasion plates catalog no. 354480), according to the manufacturer's instructions. Briefly, 125,000 cells/mL were suspended into culture

medium containing 1 μg/mL dox. Medium containing chemoattractant and 1 μg/mL dox was added to the wells of the plate; the chambers (Biocoat Matrigel chambers for invasion assays and control inserts for migration assays) were placed into the wells. 0.5 mL of the cell suspension (approximately 2.5×10^5 cells) was added into the chambers. The plates were incubated for 22 hours in 37°C in a humidified incubator with 5% CO_2. Following incubation, the media was aspirated from each well and a cotton swab was run across the surface of the chamber to remove non-invading cells. 100% methanol was added to each insert for 2 minutes to fix the cells. Then, 0.5% crystal violet was added to each insert and allowed to sit for 2 minutes. Following this step, the inserts were washed with water to remove excess stain, air dried overnight, and visualized with a light microscope at 100x magnification. Five representative images were taken from each insert and cells were manually counted using ImageJ. Data presented are the average cell numbers from the five images.

Statistical analyses

Student's t-test was used to compare differences between means of two groups. Spearman's R test was used to measure the strength of association between two variables. Two-way ANOVA test used to compare the means between two groups that were split by two independent variables. For all analyses, significance was inferred at $P < 0.05$ and P values were two-sided. Statistical analyses were performed using GraphPad Prism (GraphPad Software, Inc).

CHAPTER 3: RESULTS

Ectopic expression of FOXM1 and CCNE1 induces FOXM1 phosphorylation in FT282 cells

We hypothesized that cyclin E1 post-translationally activates FOXM1 through phosphorylation. To test this, we utilized a HGSC precursor cell model, the immortalized FTE cell line FT282 (Table 1). We engineered clonal FT282 cells (FT282-C11, hereafter referred to as FT282) (112) for dox-inducible expression of CCNE1, FOXM1c, or both (E1/F1). Importantly, western blotting revealed that only the FT282 cell line expressing both CCNE1 and FOXM1c had expression of phosphorylated FOXM1 (i.e. p-FOXM1) (Figure 8). In this western, we utilized an antibody specific for p-FOXM1 at threonine 600, a cyclin E1/CDK2 phosphorylation site in FOXM1 that was previously identified (65). To further investigate the kinetics of the phosphorylation of FOXM1, we measured p-FOXM1 at various time points by Western blot (Figure 9). In the control cell line and the cell lines overexpressing either CCNE1 or FOXM1, no phosphorylation of FOXM1 was seen, which is consistent with the above results. Induction of FOXM1 was seen around 4 hours after the addition of dox in the FOXM1 ectopic expression line (Figure 9B) and induction of CCNE1 was seen around two hours after the addition of dox in the CCNE1 ectopic expression line (Figure 9C). In the dual E1/F1 overexpressing line, CCNE1 and FOXM1 were induced at about 2 hours post dox and, importantly, p-FOXM1 was present starting at 8 hours post dox-treatment (Figure 9D).

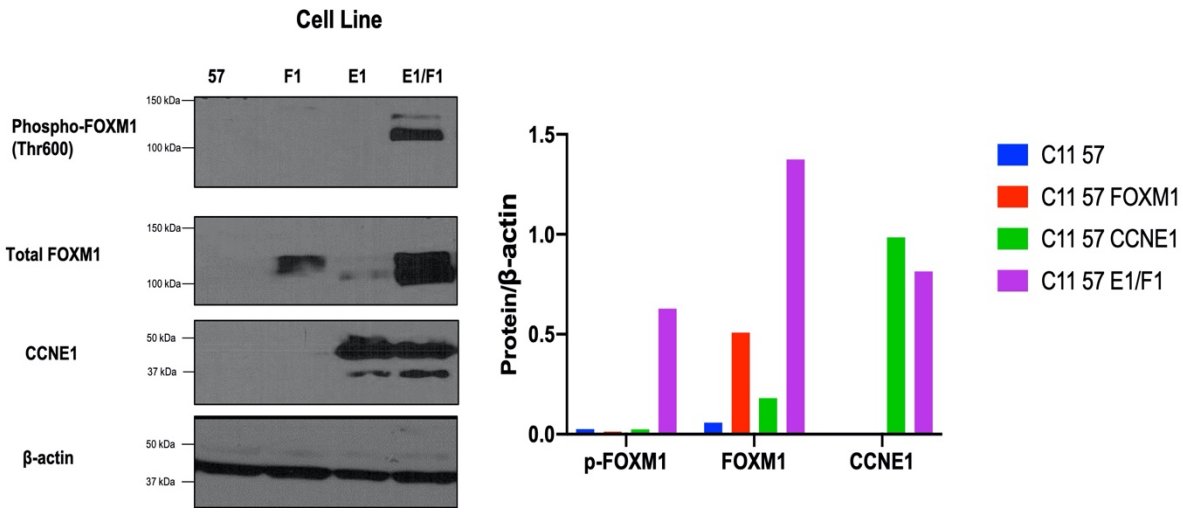

Figure 8. Phosphorylated FOXM1 is present only in FT282 cells with ectopic expression of both FOXM1 and CCNE1. Western blot analysis of p-FOXM1, total FOXM1, and CCNE1 in the FT282 cells engineered for dox-inducible empty vector control (57), FOXM1 (F1), CCNE1 (E1), or E1/F1 expression, and grown for 24 hours in the presence of 1 μg/mL dox, along with quantification of the western blot. Left: Western blot image. Right: Quantification of bands using Image J.

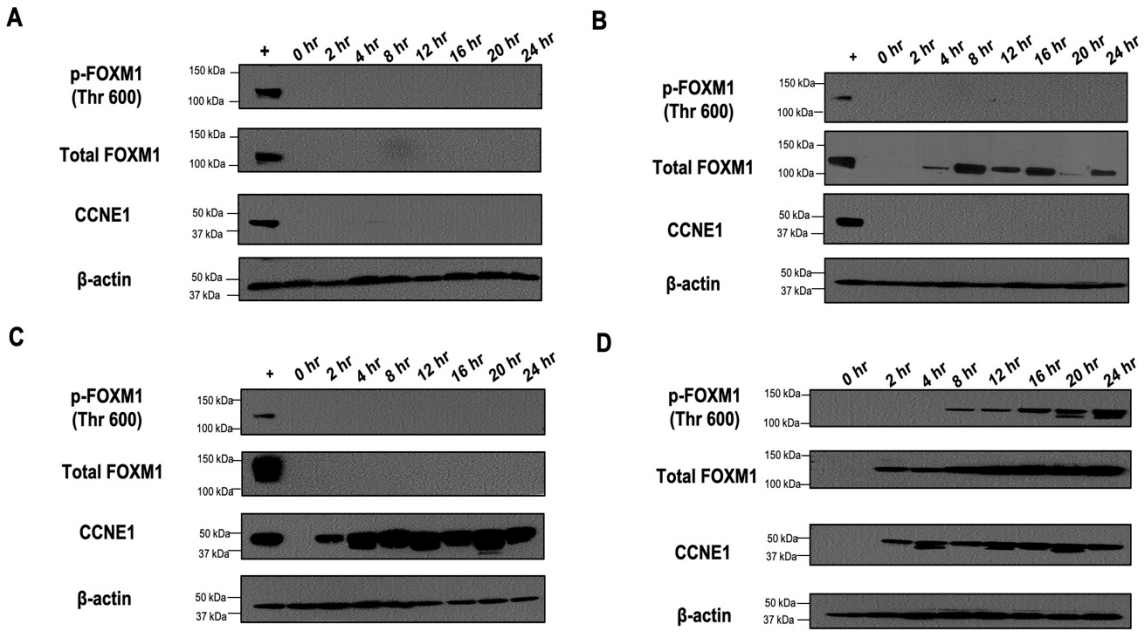

Figure 9. FOXM1 phosphorylation kinetics in engineered FT282 cells. Western blot analyses of p-FOXM1, total FOXM1, and CCNE1 in the FT282 cells engineered for dox inducible empty vector control (57), FOXM1, CCNE1, or E1/F1 expression and grown in the presence of 1 μg/mL dox. Protein was harvested at different timepoints across a 24-hour time period. **+** denotes the positive control line (E1/F1 line) **A.** C11 57 (i.e. vector control) cells, **B.** C11 57 FOXM1 cells, **C.** C11 57 CCNE1 cells, and **D.** C11 57 E1/F1 cells.

The effect of CDK inhibitors on CCNE1-dependent FOXM1 phosphorylation in FT282 cells

CCNE1 forms a complex with a cyclin dependent kinase (CDK) and causes a conformational change within the CDK, opening up the CDK active site and ATP binding pocket. Once this occurs, the complex is able phosphorylate proteins involved in cell cycle progression. Cyclin E1 most commonly complexes with CDK2, though it can complex with other CDKs, including CDK1 (103). To determine which CDK mediates cyclin E1-dependent phosphorylation of FOXM1, our experimental strategy was to initially determine the expression of CDK1 and CDK2 in FT282 cell lines, and next to treat FT282 cell lines with a panel of CDK inhibitors (CDKi) with differing target specificities (Table 3). We observed CDK1 and CDK2 protein expression in all FT282 cell lines; however, the dual expressing E1/F1 line showed slightly elevated CDK1 and CDK2 protein expression (Figure 10). FT282-CCNE1 cells also showed elevated CDK1/2 expression to a lesser extent. These elevations may be related to the stabilization of cyclin E1/CDK1/2 complexes.

Next, we treated the FT282 E1/F1 cells with dinaciclib, a well-established CDK1, 2, 5, and 9 inhibitor (Table 3). Notably, dinaciclib treatment decreased the amount of p-FOXM1, in a dose dependent manner, without substantially affecting the levels of total FOXM1 or CCNE1 (Figure 11). Next, we tested the effects of R03306, a CDK1 inhibitor. Unexpectedly, treatment of FT282 E1/F1 cells with R03306 caused an increase in p-FOXM1 without significantly impacting the levels of FOXM1, CDK2, CDK1, or CCNE1 (Figure 12). Furthermore, Palbociclib, a CDK4 and 6 inhibitor, treatment did not impact the levels of p-FOXM1, or of total FOXM1, CDK2, CDK2, or CCNE1 levels (Figure 13). Finally, treatment of the FT282 E1/F1 cells with AT7519, a CDK 1, 2, 4, 6 and 9 inhibitor, led to a decrease in p-FOXM1 levels (Figure 14). Taken together, the results of these

experiments suggest that CDK2 is the chief CDK responsible for CCNE1-mediated FOXM1 phosphorylation in FT282 cells (Table 3)

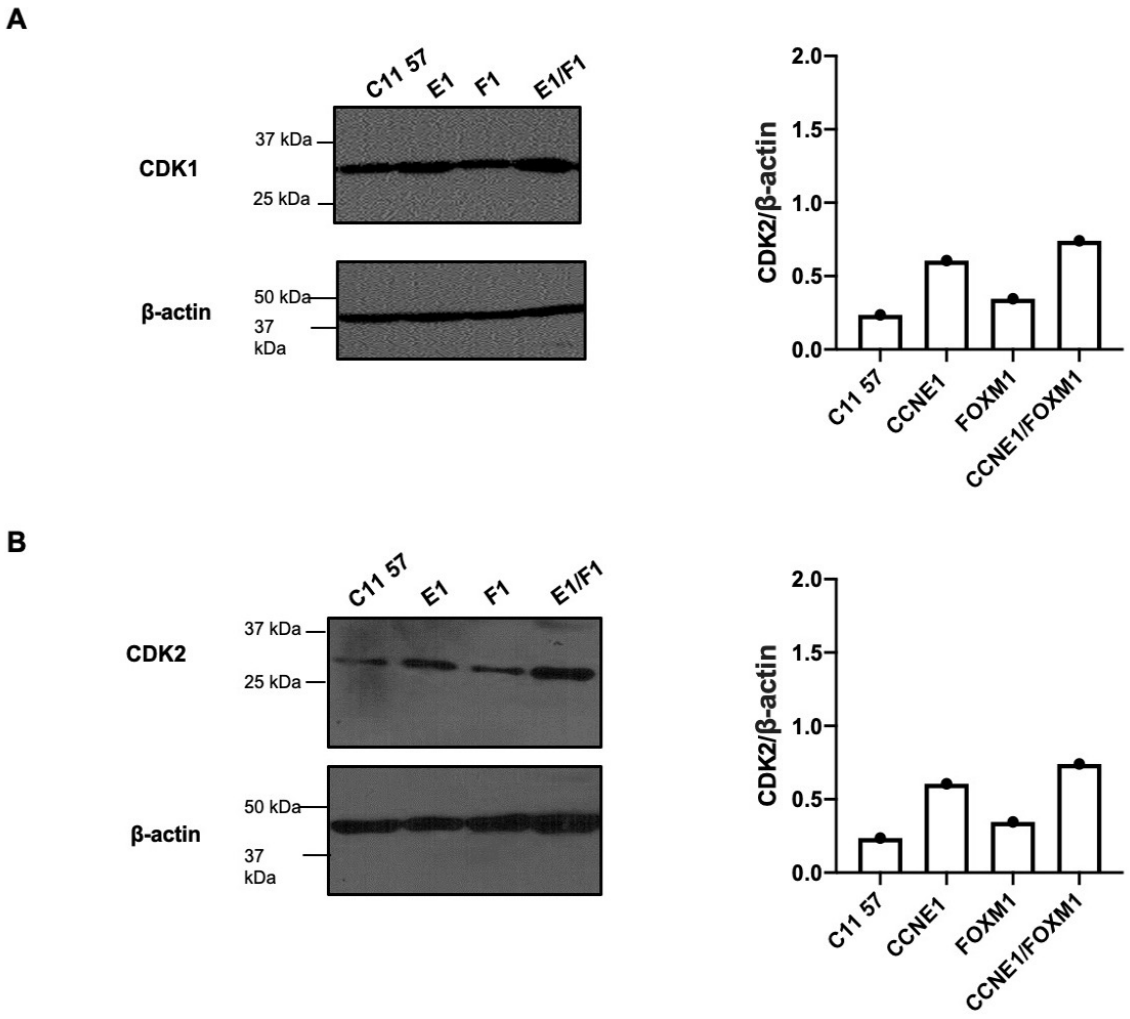

Figure 10. CDK1 and CDK2 protein expression in FT282 cell lines. Western blot analysis of CDK1 and CDK2 in the FT282 cells engineered for dox-inducible empty vector control (57), FOXM1, CCNE1, or E1/F1 expression and grown for 24 hours in the presence of 1 μg/mL dox. **A.** Western blot probing for CDK1 on the left, with the Image J protein quantification on the right, and **B.** Western blot probing for CDK2 on the left, with Image J protein quantification on the right.

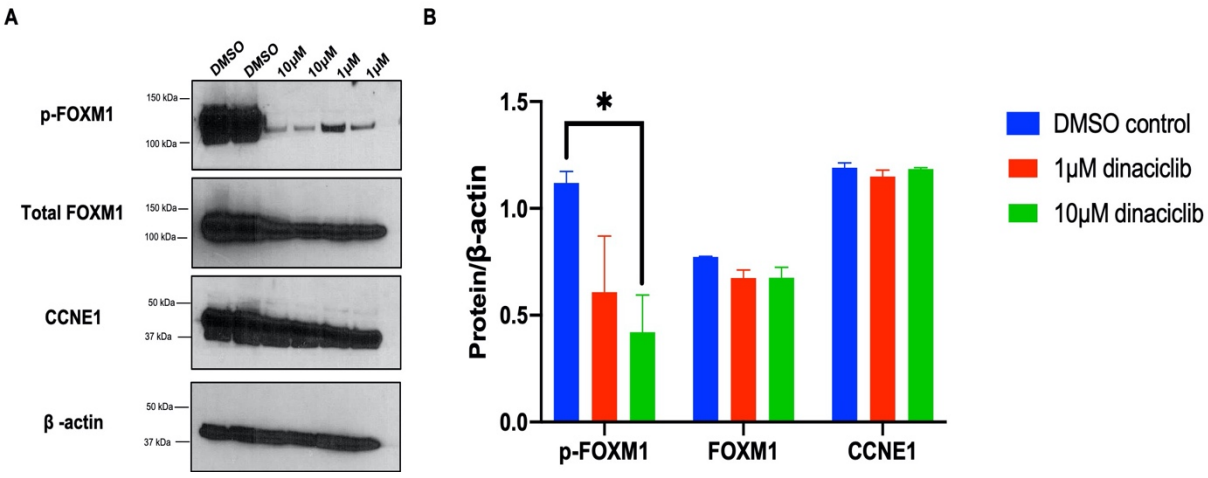

Figure 11. Treatment of FT282 E1/F1 cells with dinaciclib results in a decrease of p-FOXM1. Western blot analysis of p-FOXM1, total FOXM1, and CCNE1 in the FT282 cells engineered for dox inducible E1/F1 expression. Cells were grown for 24 hours in the presence of 1 μg/mL dox, then treated with dinaciclib in 10 μM and 1 μM concentrations. 24 hours after drug treatment, whole cell proteins were harvested and a western blot analysis conducted. **B.** Quantification of the western blot analysis. Treatment of cells, protein extraction, and western blotting were repeated twice. Bars represent mean ± SD. Significant student's *t* test *p* values are shown. *P* value designation: * < 0.05. All other comparisons were not significant.

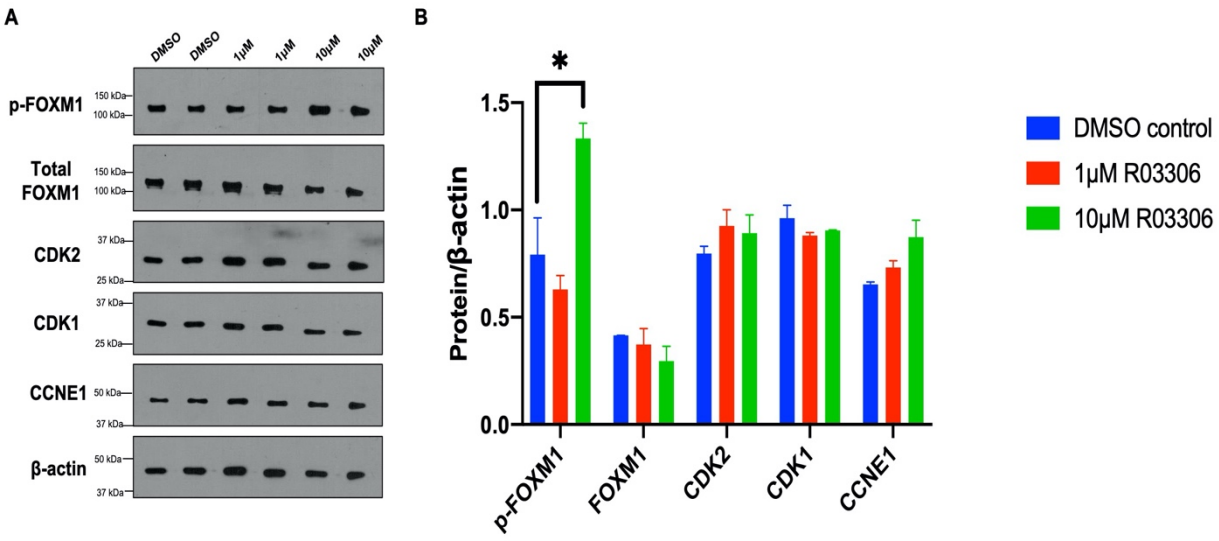

Figure 12. Treatment of FT282 E1/F1 cells with R03306 results in an increase of p-FOXM1. A. Western blot analysis of p-FOXM1, total FOXM1, CDK2, CDK1, and CCNE1 in the FT282 cells engineered for dox inducible E1/F1 expression. Cells were grown for 24 hours in the presence of 1 μg/mL dox, then treated with R03306 in 10 μM and 1 μM concentrations. 24 hours after drug treatment, whole cell protein was harvested and a western blot analysis conducted. **B.** Quantification of the western blot analysis. Treatment of cells, protein extraction, and western blotting were repeated twice. Bars represent mean ± SD. Significant student's *t* test *p* values are shown. *P* value designation: * < 0.05. All other comparisons were not significant.

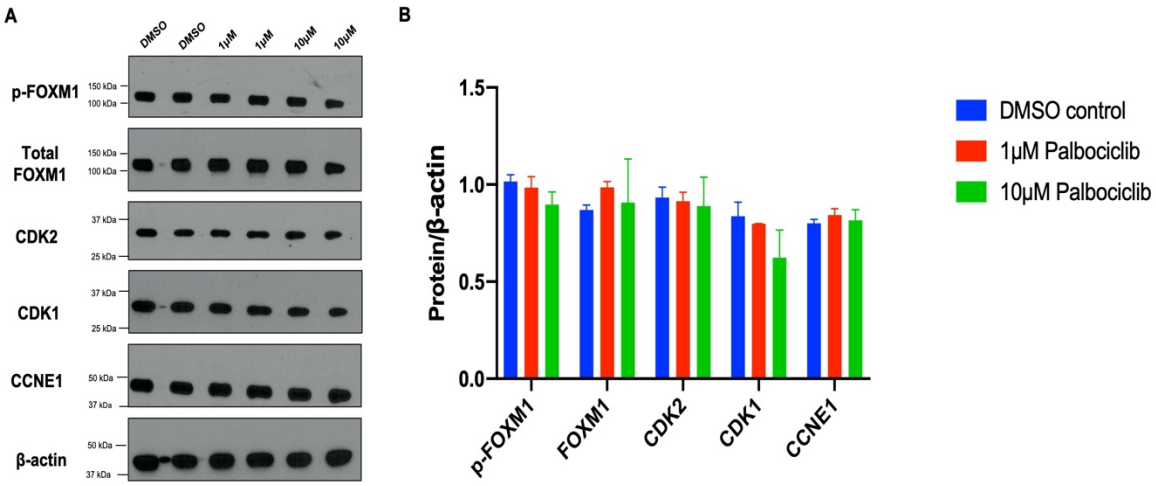

Figure 13. Treatment of FT282 E1/F1 cells with Palbociclib does not alter p-FOXM1 levels. A. Western blot analysis of p-FOXM1, total FOXM1, CDK2, CDK1, and CCNE1 in the FTE cells engineered for dox inducible E1/F1 expression. Cells were grown for 24 hours in the presence of 1 μg/mL dox, then treated with Palbociclib in 10 μM and 1 μM concentrations. 24 hours after drug treatment, whole cell proteins were harvested and used for western blot analysis. **B.** Quantification of the western blot data using Image J. Treatment of cells, protein extraction, and western blotting were repeated twice. Bars represent mean ± SD. Student's *t* test performed, all comparisons were not significant.

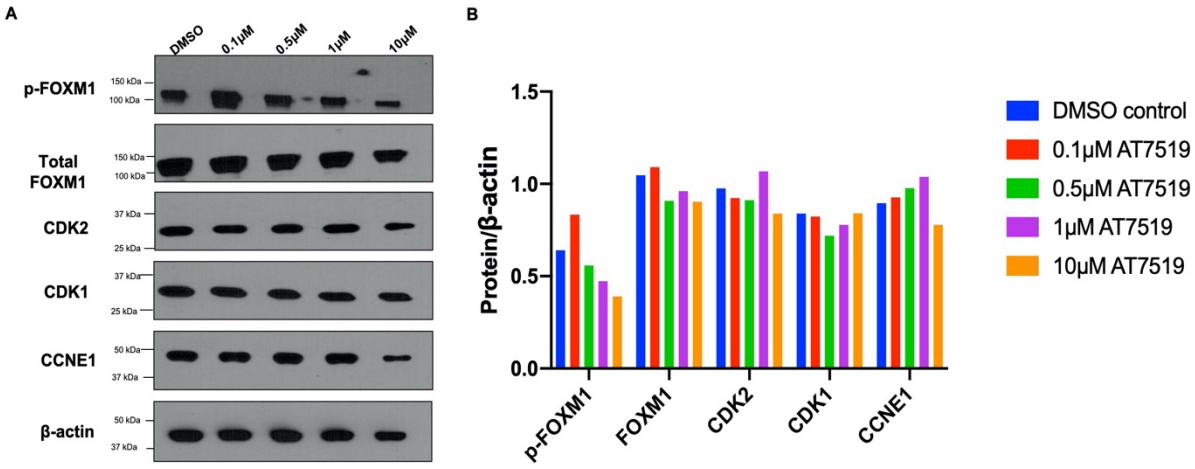

Figure 14. Treatment of FT282 E1/F1 cells with AT7519 results in a decrease in p-FOXM1. A. Western blot analysis of p-FOXM1, total FOXM1, CDK2, CDK1, and CCNE1 in the FT282 cells engineered for dox inducible CCNE1/FOXM1 expression. Cells were grown for 24 hours in the presence of 1 μg/mL dox, then treated with AT7519 in 0.1, 0.5, 1, and 10 μM concentrations. 24 hours after drug treatment, whole cell protein was harvested and a western blot analysis conducted. **B.** Quantification of the western blot analysis.

CDK inhibitor	References	CDK specificity	Effect on p-FOXM1
Dinaciclib	113, 114	CDK1, 2, 5, and 9	Decrease
R03306	115	CDK1	Increase
Palbociclib	116	CDK4 and 6	No change
AT-7519	117, 118	CDK1, 2, 4, 6, and 9	Decrease

Table 3. CDK inhibitor specificity and effect on p-FOXM1 levels in FT282 E1/F1 cells. The references for each inhibitor indicates the original study in which the CDK inhibitor was discovered and the study determining the inhibitor's CDK specificity, if applicable. The effect on p-FOXM1 was determined in the current study (see Figures 11-14).

p-FOXM1, total FOXM1, CCNE1, and CDK2 protein expression in HGSC lines

Next, we determined the levels of p-FOXM1, total FOXM1, and CCNE1 in clinically relevant cell line models of human HGSC. All the cell lines have *Tp53* mutations and heterogeneous alterations in *CCNE1* and *FOXM1* pertinent to HGSC (Table 4). In total, we surveyed nine human HGSC cell lines. We found that cyclin E1 was expressed in the majority of the HGSC lines and was localized to both the cytoplasm and nucleus (Figures 15 and 16). CDK2 showed a similar pattern to cyclin E1, as it was expressed in the majority of the HGSC cell lines and tended to show expression in both the cytoplasm and nucleus. In contrast, total FOXM1 was expressed in all HGSC lines but was present primarily in the nucleus (Figures 15 and 16). Importantly, phosphorylated FOXM1 was detected in all HGSC cell lines and was present primarily in the nucleus (Figures 15 and 16). These data suggest that activated FOXM1 is a common phenotype of HGSC cell lines.

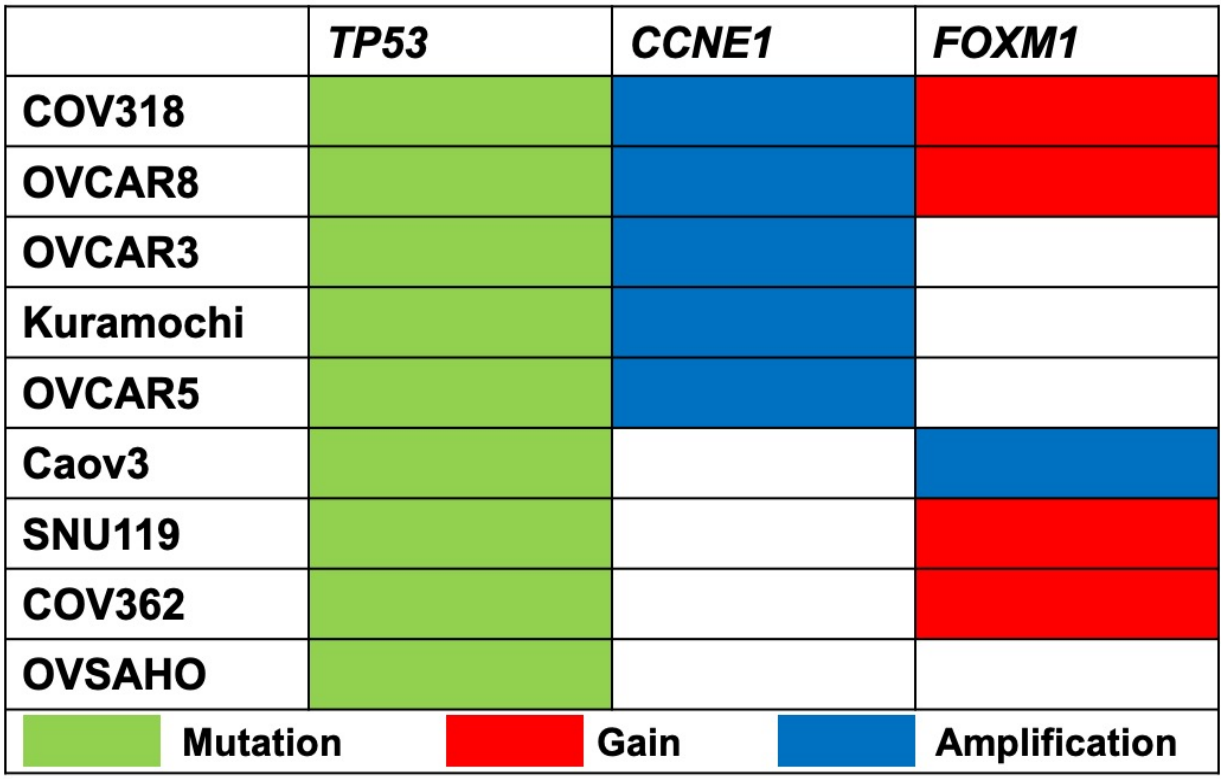

Table 4. HGSC cell line genomic characteristics. TP53 indicates somatic mutation of the *Tp53* gene. Gene gain and amplification of *FOXM1* was determined by GISTIC (43,119). *CCNE1* gain and amplification information was obtained from cBioPortal and (120). In GISTIC, a numerical value of 0 indicates a diploid cell line, +1 indicates a low-level gain (a few additional copies of the gene), and a value of +2 indicates a high-level amplification.

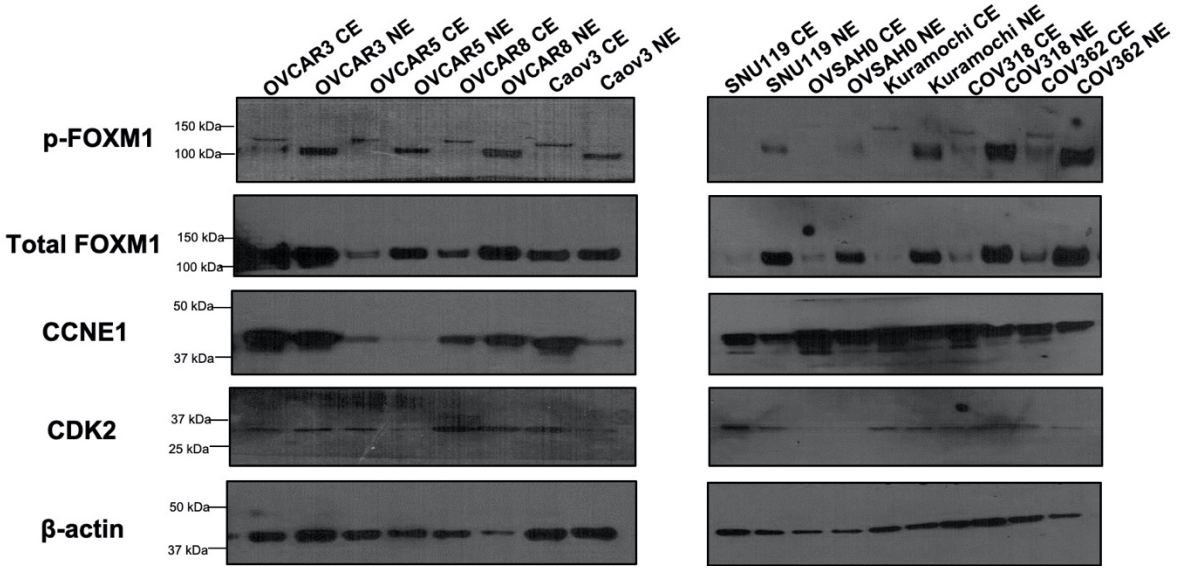

Figure 15. p-FOXM1, total FOXM1, CCNE1, and CDK2 protein expression in HGSC cell lines. Western blot analysis of p-FOXM1, total FOXM1, CCNE1, and CDK2 in HGSC cell lines. Nuclear and cytoplasmic extracts were harvested 24 hours post seeding. **CE: cytoplasm extract, NE: nuclear extract**

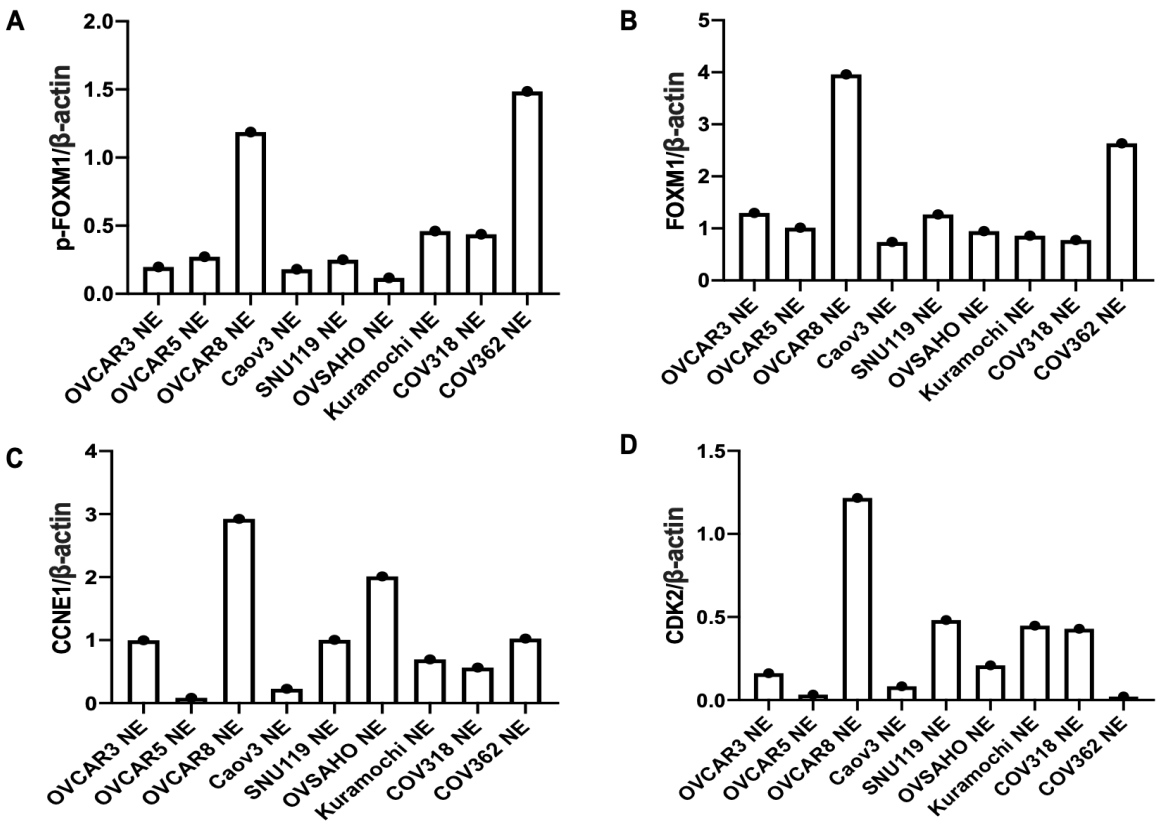

Figure 16. Quantification of the levels of p-FOXM1, total FOXM1, CCNE1, and CDK2 proteins in HGSC cell line nuclear extracts. Quantification of the Western blot analyses of p-FOXM1, total FOXM1, CCNE1, and CDK2 in a HGSC cell line panel. Nuclear and cytoplasmic extracts were harvested 24 hours post seeding. **A.** Quantification of p-FOXM1 in nuclear extracts obtained from HGSC cell lines, **B.** Quantification of total FOXM1 in the nuclear extracts of the HGSC cell lines, **C.** Quantification of CCNE1 in the nuclear extracts of the HGSC cell lines and, **D.** Quantification of CDK2 in the nuclear extracts of the HGSC cell lines.

p-FOXM1, total FOXM1, CCNE1, and CDK2 protein expression in primary EOC tumor samples

We next examined the expression patterns of the aforementioned proteins in primary EOC tumors (Figure 17). We performed western blot analyses on whole cell extracts from 43 tumor samples and used bulk normal ovary (NO) as a control tissue. Interestingly, these proteins showed widespread but heterogeneous expression in primary EOC (Figure 17). Next, to determine whether expression of the individual proteins correlate, we quantified target band intensities using Image J, and performed statistical correlation analyses. Notably, we found that the expression of all protein pairs tested showed highly significant correlations. The strongest correlations were between CDK2 and cyclin E1, followed by p-FOXM1 and CDK2 and p-FOXM1 and cyclin E1. A moderately lower but still highly significant correlation was seen between p-FOXM1 and FOXM1, FOXM1 and CDK2, and FOXM1 and cyclin E1 (Figure 18). A summary of the comparisons and corresponding Spearman correlations is presented in Table 5. To further illustrate the degree of protein correlations, we arranged protein expression in the tumors by descending p-FOXM1 tumor expression. As shown in Figure 19, there was a similar decreasing protein expression pattern observed for total FOXM1, cyclin E1, and CDK2.

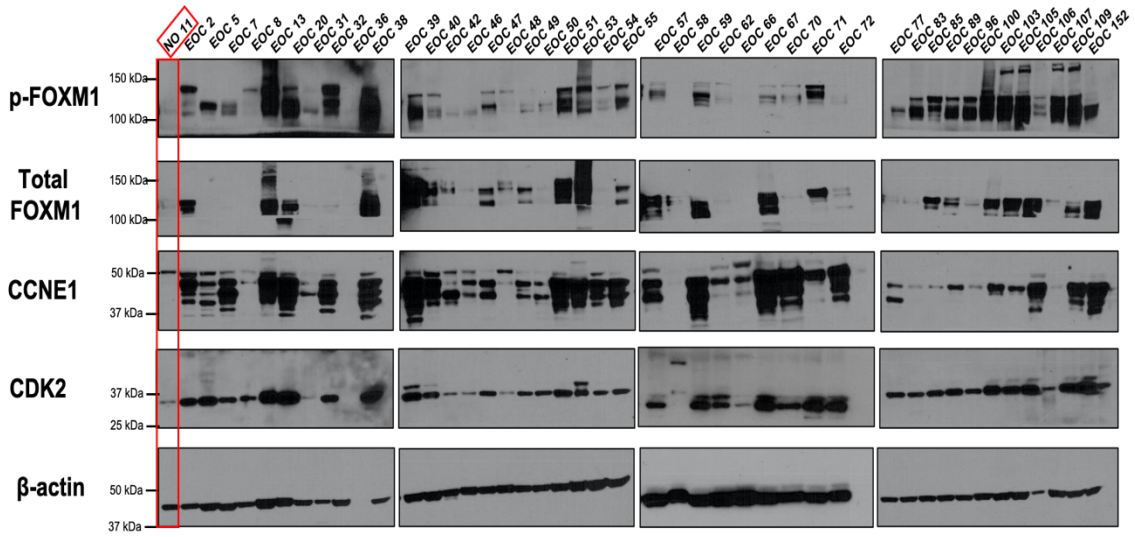

Figure 17. Western blot analyses of p-FOXM1, total FOXM1, cyclin E1, and CDK2 expression in normal ovary and primary EOC tumor samples. Western blot analyses of whole cell extracts for p-FOXM1, cyclin E1, and CDK2 in primary tumor samples obtained from patients undergoing surgical resection at RPCCC. NO is a bulk normal ovary sample that serves as a control and is denoted by the red outlined box. EOC are epithelial ovarian cancer samples and the number is the patient identification number. We surveyed a total of 43 EOC samples.

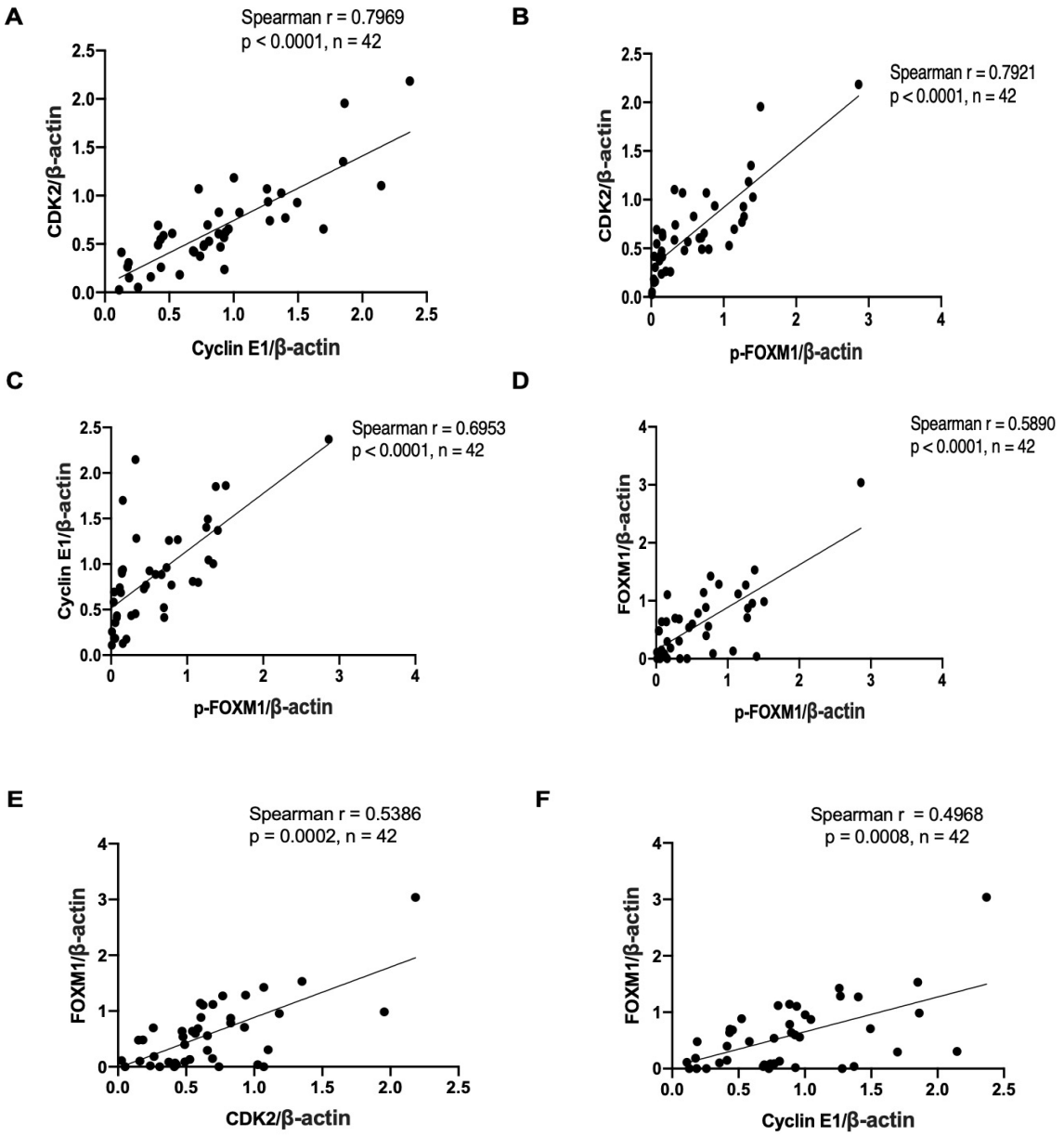

Figure 18. Correlations between p-FOXM1, total FOXM1, CCNE1, and CDK2 protein expression in primary EOC tumor samples. Spearman correlation analyses were performed using western blot data from primary EOC samples obtained from patients undergoing surgical resection at RPCCC (Figure 18). **A.** Cyclin E1 vs. CDK2. **B.** CDK2 vs. p-FOXM1. **C.** Cyclin E1 vs, p-FOXM1. **D.** FOXM1 vs. p-FOXM1 protein levels. **E.** CDK2 vs. FOXM1. **F.** Cyclin E1 vs. FOXM1. Target protein expression was normalized to β-actin prior to performing the correlation analysis.

Comparison	Spearman Coefficient	p-value	Sample size
CDK2 vs. Cyclin E1	0.7969	p < 0.0001	n = 42
CDK2 vs. p-FOXM1	0.7921	p < 0.0001	n = 42
Cyclin E1 vs. p-FOXM1	0.6953	p < 0.0001	n = 42
FOXM1 vs. p-FOXM1	0.5890	p < 0.0001	n = 42
FOXM1 vs. CDK2	0.5386	p = 0.0002	n = 42
FOXM1 vs. Cyclin E1	0.4968	p = 0.0008	n = 42

Table 5. Spearman correlations between p-FOXM1, total FOXM1, cyclin E1, and CDK2 protein expression in primary EOC tumor samples. Data were obtained from western blotting of whole cell extracts. Protein comparisons are listed in descending order of Spearman coefficients.

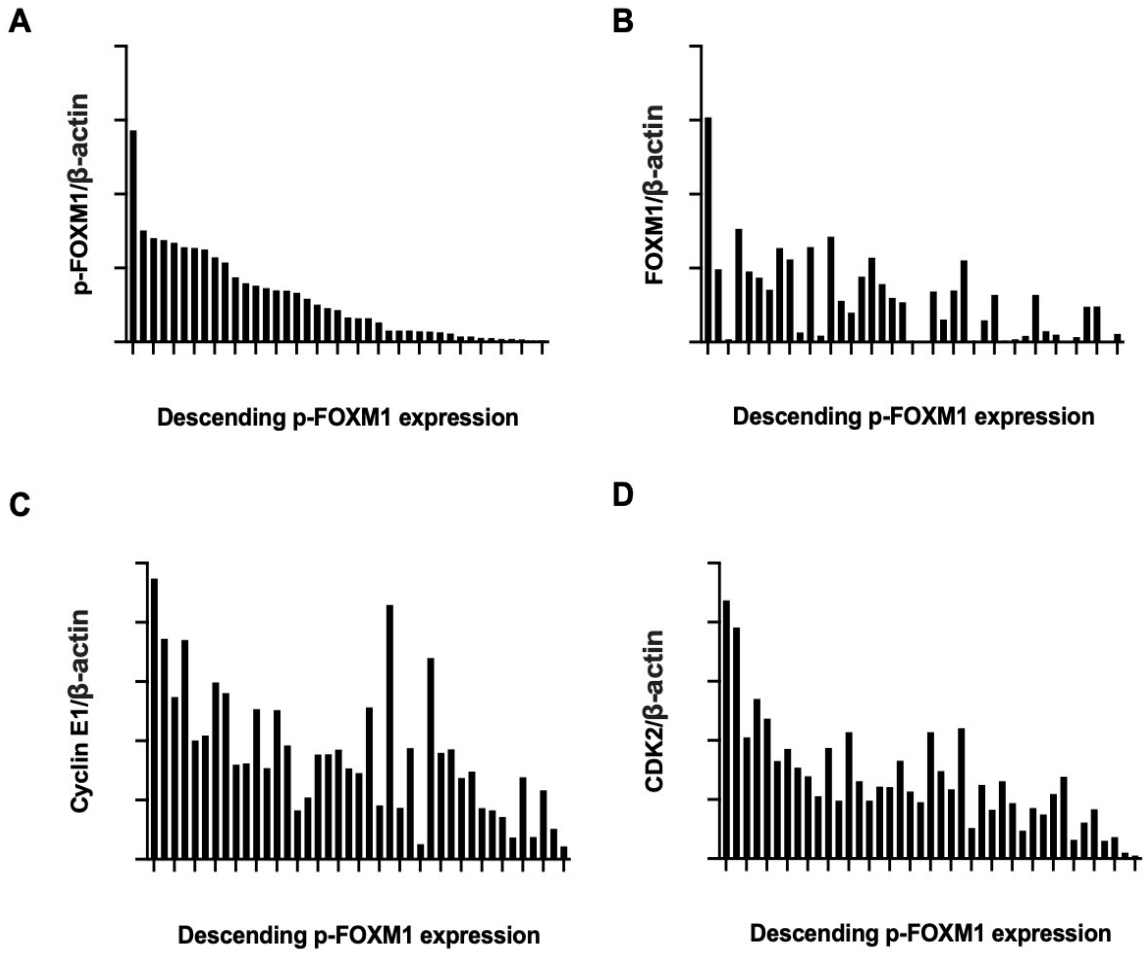

Figure 19. p-FOXM1, total FOXM1, cyclin E1, and CDK2 protein expression in primary EOC samples, arranged in descending order of p-FOXM1 expression. Data obtained through quantification of western blot analyses of primary EOC samples obtained from patients undergoing surgical resection at RPCCC. **A.** p-FOXM1, **B.** total FOXM1, **C.** Cyclin E1, and **D.** CDK2. Protein expression levels are displayed in order of descending p-FOXM1 expression.

Dinaciclib treatment reduces the levels of phosphorylated FOXM1 in OVCAR8 HGSC cells

Next, we determined the effect of dinaciclib treatment on p-FOXM1 levels in OVCAR8 cells. Dinaciclib was chosen based on its robust inhibitory effect observed in the FT282 cell model (Figure 11). In addition, we chose OVCAR8 as a cell model because it showed high expression of the proteins under examination (p-FOXM1, total FOXM1, CCNE1, and CDK2) (Figures 15 and 16). Notably, dinaciclib treatment profoundly affected the levels of p-FOXM1 and CDK2 in OVCAR8 nuclear extracts, decreasing p-FOXM1 levels two-fold and CDK2 levels ten-fold (Figure 20). Additionally, the nuclear levels of total FOXM1 and cyclin E1 also decreased with dinaciclib treatment (Figure 20).

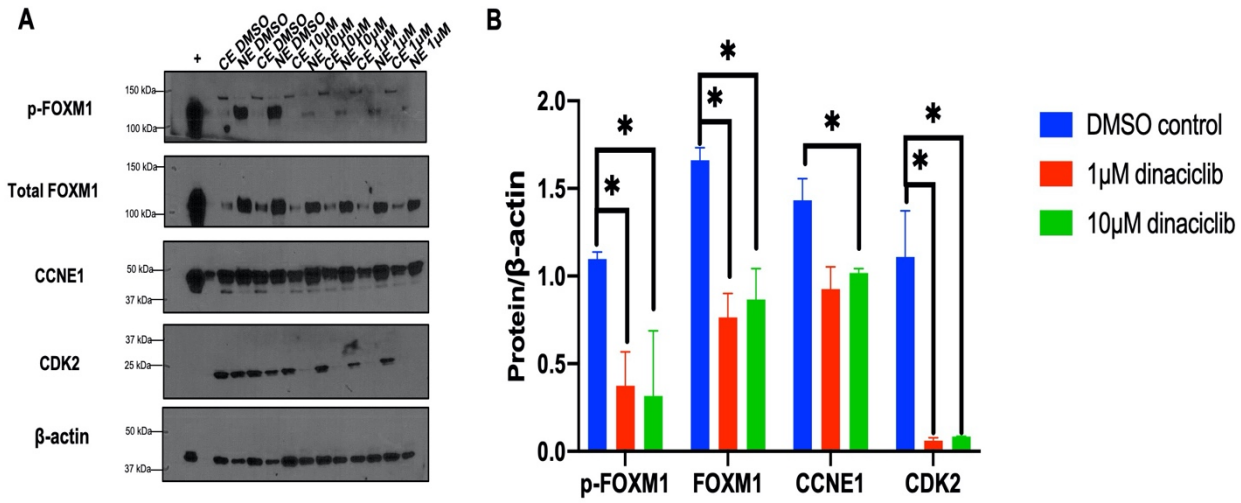

Figure 20. Treatment of OVCAR8 cells with dinaciclib results in a decrease of p-FOXM1. A. Western blot analyses of p-FOXM1, total FOXM1, Cyclin E1, and CDK2 in the OVCAR8 HGSC cell line. Cells were seeded in duplicate and treated 24 hours post seeding with Dinaciclib (10 μM and 1 μM concentrations) and a DMSO control. Nuclear (NE) and cytoplasmic extracts (CE) were harvested 24 hours after drug treatment. The positive control was the FT282 E1/F1 cells and is denoted by a +. **B.** Quantification of the p-FOXM1, total FOXM1, cyclin E1, and CDK2 protein expression levels in OVCAR8 nuclear extracts. Bars represent mean ± SD. Significant student's *t* test *p* values are shown. *P* value designation: * < 0.05.

Transformation characteristics of FT282 cells engineered for ectopic expression of CCNE1, FOXM1 or both proteins.

Next, to determine what phenotypic role ectopic expression of FOXM1 and CCNE1 may play in HGSC oncogenesis, we measured transformation characteristics using engineered FT282 cells. Supporting these investigations, both CCNE1 and FOXM1 are expressed in pre-neoplastic lesions in the distal FTE (39, 83). Utilizing the FT282 model system, we measured cell proliferation, migration, invasion, and clonogenic growth characteristics.

Cell proliferation assays revealed that the dually expressing E1/F1 FT282 cell line has increased proliferation in comparison to the empty vector control or singly expressing (E1 or F1) lines (Figure 21). The empty vector cells grew the slowest, with the singly expressing lines displaying similar trajectories of growth that were significantly greater than the vector control.

Cell migration assays revealed that the E1/F1 cells migrated most efficiently, followed by FOXM1 expressing cells, CCNE1 expressing cells, and vector control cells (Figure 22). Furthermore, the invasive properties of the cell lines was highly similar to the migratory capacity (Figure 23). Finally, all ectopic expression cell lines showed clonogenic growth that was highly elevated over vector control cells, but the individual lines were each similar (Figure 24).

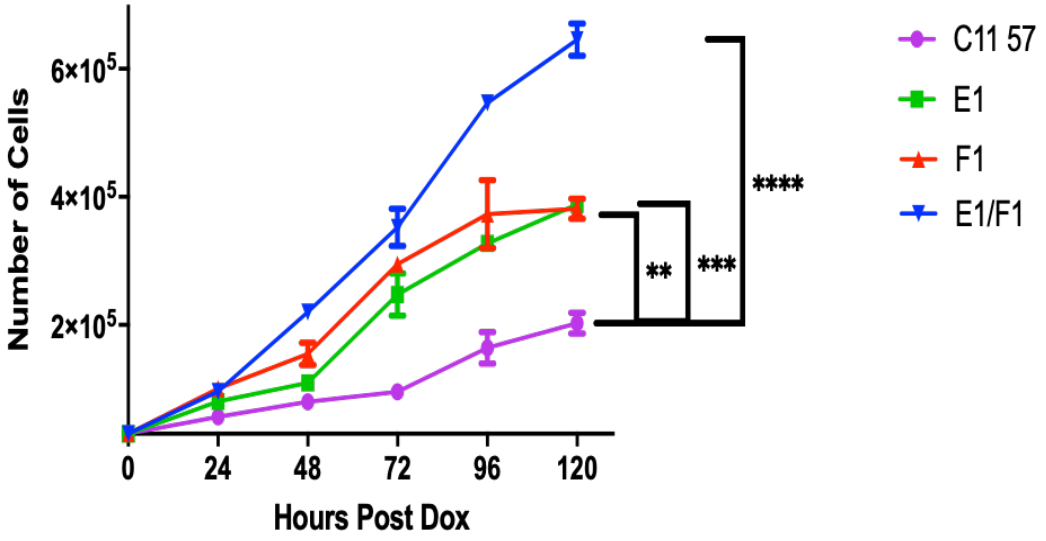

Figure 21. E1/F1 ectopic expression FT282 cells show a higher proliferation rate than FOXM1 or CCNE1 expressing cells. FT282 cells engineered for dox inducible empty vector control (57), FOXM1, CCNE1, or E1/F1 expression were seeded at a density of 20,000 cells per well into 6-well plates, seeding each cell line in triplicate. A plate was seeded for each day of counting. 24 hours post seeding, the media was replaced with media containing 1 µg/mL dox. The media with dox was replenished every 48 hours. The following procedure was used to count the cells: the wells were washed with room temperature PBS, trypsinized, centrifuged at 500g for five minutes, resuspended in one mL of media, and counted using a Bio Rad TC20 automated cell counter. Total cells were counted every 24 hours for 5 days. Bars represent mean ± SD. Two-way ANOVA *p* values are shown. *P* value designations: **** < 0.0001, *** < 0.001, ** < 0.01.

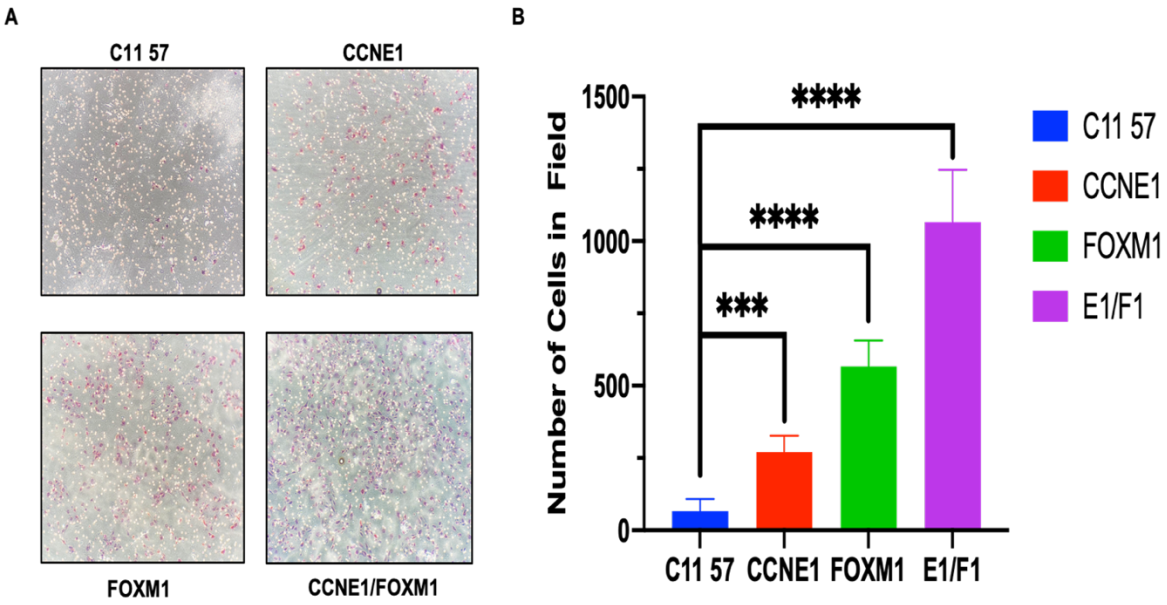

Figure 22. E1/F1 ectopic expression FT282 cells show higher rates of cell migration compared to FT282 cells with CCNE1 or FOXM1 expression alone. A Corning migration assay was performed on FT282 cells engineered for dox-inducible empty vector control (57), FOXM1, CCNE1, or E1/F1 expression. Approximately 250,000 cells suspended in media containing 1 µg/mL dox were added into control chambers. The chambers were placed into wells containing media with chemoattractant and 1 µg/mL of dox. After 22 hours of incubation, the chambers were fixed with 100% methanol, stained with 0.5% crystal violet, and visualized with a light microscope at 100x magnification. **A.** Representative images of the migration assay in the indicated FT282 cells. Purple stained cells indicate cells that have migrated through the control insert, white circles indicate pores. **B.** Quantification of migrated cells in the FT282 cell lines (n=5). Bars represent mean ± SD. Student's *t* test *p* values are shown. *P* value designations: **** < 0.0001, *** < 0.001.

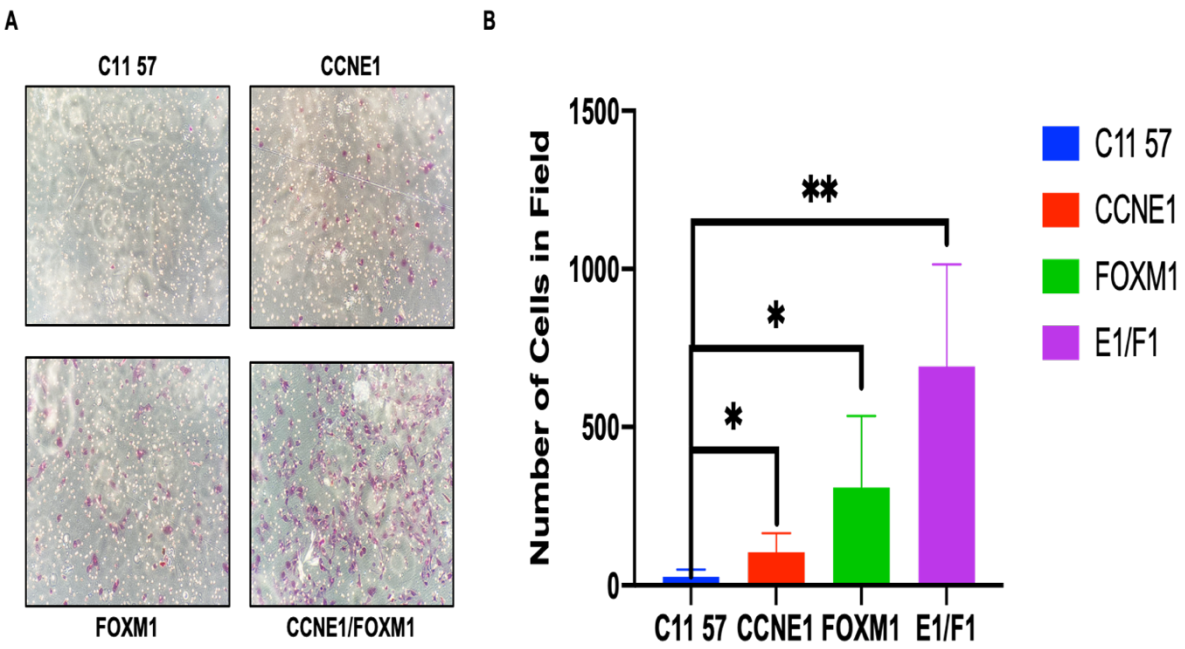

Figure 23. E1/F1 ectopic expression FT282 cells show higher rates of invasion compared to FT282 cells with CCNE1 or FOXM1 expression alone. A Corning Biocoat Matrigel assay was performed on the FT282 cells engineered for dox-inducible empty vector control (57), FOXM1, CCNE1, and E1/F1 expression. Approximately 250,000 cells suspended in media containing 1 µg/mL of dox were added into Biocoat Matrigel chambers. The chambers were placed into wells containing media with chemoattractant and 1 µg/mL dox. After 22 hours of incubation, the chambers were fixed with 100% methanol, stained with 0.5% crystal violet, and visualized with a light microscope at 100x magnification. **A.** Representative images of the invasion assay in the FT282 cell lines. Purple stained cells indicate cells that have invaded through the Matrigel insert, white circles indicate pores. **B.** Quantification of migrated cells in the FT282 cell lines (n=5). Bars represent mean ± SD. Student's *t* test *p* values are shown. *P* value designations: ** < 0.01, * < 0.05.

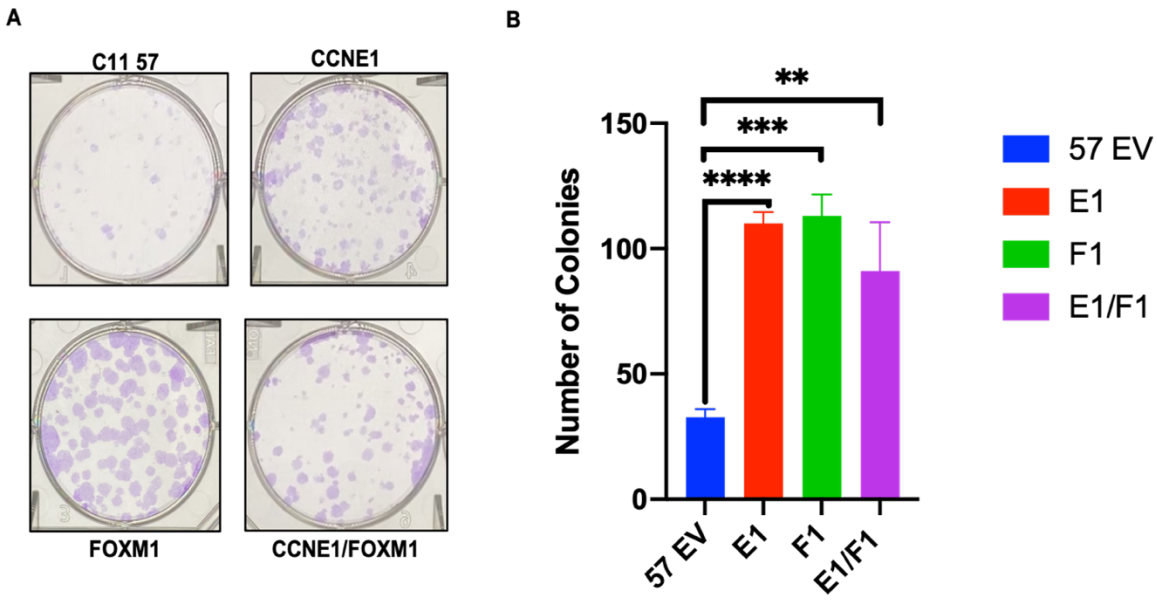

Figure 24. Clonogenic growth (i.e. colony formation) assay of FT282 cells with ectopic CCNE1, FOXM1, or E1/F1 expression. A. FT282 cells engineered for dox-inducible empty vector control (57), FOXM1, CCNE1, and E1/F1 expression. were seeded into 6-well plates, in triplicate, at a density of 500 cells per well. 1 µg/mL of dox was added to the media 24 hours post seeding and was replenished every 48 hours. Colony formation was measured after eight days, and the cells were fixed in methanol and stained with crystal violet. **B.** Colonies containing greater than 50 cells were counted and clonogenic survival was quantified as an average of three replicates. Bars represent mean ± SD. Student's *t* test *p* values are shown. *P* value designations: **** < 0.0001, *** < 0.001, ** < 0.01. Experiments were repeated five times.

CHAPTER 4: DISCUSSION

FOXM1 pathway activation is the second most common molecular alteration in HGSC, after Tp53 mutation, and *CCNE1* is amplified and overexpressed in 20% of HGSC cases. Both FOXM1 and cyclin E1 have been extensively studied in cancer, but the potential interaction of the two proteins in HGSC progression, or in any other cancer model system, has not previously been addressed. A previous study showed that CCNE1/CDK2 complexes phosphorylate FOXM1 and identified 3 amino acid residues within the FOXM1 protein that are CCNE1/CDK2 phosphorylation sites (65). The phosphorylation of FOXM1 is critical, as phosphorylation results in functional activation of FOXM1 as a transcription factor. Moreover, we previously reported strong correlations between FOXM1 and CCNE1/Cyclin E1 mRNA and protein expressions in TCGA data, and showed that ectopic expression of CCNE1 in FTE cells resulted in increased FOXM1 expression (43). Further investigation into the CCNE1/CDK and FOXM1 interaction in the context of HGSC has not been investigated and provided the impetus for our studies.

Herein, we report several key findings relevant to CCNE1/CDK and FOXM1 and their functional interactions in HGSC: **1.** Expression of p-FOXM1 was seen only in the CCNE1 and FOXM1 dual expression cell line. **2.** CCNE1 and FOXM1 are expressed prior to p-FOXM1 expression in the dual expression CCNE1 and FOXM1 FTE line. **3.** CDK1 and CDK2 are both expressed in the FT282 cell models, however drug treatments with CDK inhibitors implicate CDK2 as the primary CDK that mediates cyclin E1-mediated phosphorylation of FOXM1. **4.** p-FOXM1, total FOXM1, cyclin E1, and CDK2 are all expressed in HGSC cell lines, with p-FOXM1 and FOXM1 localized primarily to the nucleus. **5.** Treatment with a CDK inhibitor (dinaciclib) decreases p-FOXM1 nuclear levels in a HGSC cell line. **6.** p-FOXM1, total FOXM1, CCNE1, and CDK2 are expressed

in primary EOC tumor samples, and each of the protein pairs show strongly correlated expression. **7.** Ectopic expression of CCNE1 and FOXM1 drives key transformative phenotypes in FT282 cells including cell proliferation, migration, invasion, and clonogenic growth. Critically, for all but one of the assessed phenotypes, dual expression cells showed significantly stronger transformative properties than did single ectopic expression cells.

Three CCNE1/CDK2 phosphorylation sites in FOXM1 were reported previously (65). We confirmed that one of these phosphorylation sites (threonine 600) is phosphorylated as a result of the formation of the CCNE1/CDK complex in FTE cells, as the p-FOXM1 species was observed in only the CCNE1/FOXM1 overexpressing FTE cell line. p-FOXM1 is also detected at a later timepoint, after both CCNE1 and FOXM1 are expressed. Therefore, the formation of p-FOXM1 occurs only in the dually expressing line, and it is contingent upon the earlier production and accumulation of sufficient levels of both FOXM1 and cyclin E1.

We investigated the impact of CDK inhibitors on phosphorylation of FOXM1. Dinaciclib shows promise as a cancer drug and has been used in both Phase II and Phase III clinical trials in various cancers, with promising results in the treatment of lymphomas and leukemia (121, 122, 123). We confirmed that both CDK1 and CDK2 are expressed in FT282 cell lines, with a slight increase in expression in CCNE1 overexpressing and CCNE1/FOXM1 overexpressing lines. After treating the FT282 E1/F1 line with dinaciclib, we observed a profound reduction in p-FOXM1. There is evidence in the literature that CDK1 can compensate for loss of CDK2, so confirmation of CDK2 as the primary partner with CCNE1 was needed (103). As a CDK2 selective inhibitor is not currently available, we utilized additional CDK inhibitors with differing specificities: R03306 (CDK1 inhibitor), Palbociclib (CDK4 and 6 inhibitor), and AT7519 (CDK1, 2, 4, 6, and 9) (Table 3). To test the role of CDK1 in the CCNE1-mediated

phosphorylation of FOXM1, we used R03306, a CDK1 inhibitor. Interestingly, R03306 caused an unexpected increase in p-FOXM1 levels in FT282 E1/F1 cells. We speculate that CDK1 may complex with CCNE1 and once CDK1 is blocked by this drug, a compensatory mechanism comes into play. A potential mechanism is that when CDK1 is unable to bind with CCNE1, more CCNE1 is available for binding with CDK2, and this results in increased phosphorylation of FOXM1. In this scenario, CDK1/CCNE1 may not target FOXM1 for phosphorylation, may target a distinct site on FOXM1 not recognized by our antibody, or may be significantly less efficient than CDK2/CCNE1 complexes for targeting FOXM1.

To further confirm that CDK2 is the main binding partner of CCNE1 that mediates phosphorylation of FOXM1, we treated FT282 E1/F1 cells with Palbociclib (a CDK4 and 6 inhibitor) and AT7519 (a CDK1, 2, 4, 6, and 9 inhibitor). We expected little to no decrease in FOXM1 phosphorylation with Palbociclib treatment, as it targets CDK4 and 6, and this is indeed what we observed. Conversely, we expected a decrease of p-FOXM1 when AT7519 was used. As expected, AT7519 treatment led to a decrease in p-FOXM1, lending further support to the hypothesis that CDK2 may be the main CDK complexing with CCNE1 to phosphorylate FOXM1. In the future, generation of CDK1 and CDK2 knockdown cell lines may help further elucidate the nature of CCNE1-mediated FOXM1 phosphorylation. This knowledge may be therapeutically relevant, as it will aid in drug selection to impair FOXM1 function in HGSC. Furthermore, we can't rule out CDK9 as a potential CDK in the CCNE1-mediated phosphorylation of FOXM1. Both CDK inhibitors that showed a reduction in p-FOXM1, dinaciclib and AT7519, block CDK9. There is no literature that supports CCNE1 complexing with CDK9, but usage of a CDK9 specific inhibitor would verify that the phosphorylation of FOXM1 is not through a CCNE1 and CDK9 complex.

To further confirm the relevance of the CCNE1 and FOXM1 interaction in ovarian

cancer, we determined the levels of p-FOXM1, FOXM1, cyclin E1, and CDK2 in a panel of HGSC cancer cell lines. We found that p-FOXM1, FOXM1, cyclin E1, and CDK2 were all present in the cancer cell lines, with FOXM1 located primarily in the nucleus. These data indicate that in HGSC lines, the principal proteins relevant to FOXM1 activation are present. Importantly, we also observed that FOXM1 is activated in many HGSC cell lines, as indicated by its nuclear localization and by the detection of p-FOXM1 in the nucleus, with phosphorylation at residue threonine 600. The copy number of *FOXM1* and *CCNE1* did not appear to correlate well with the respective protein expression in HGSC cell lines (data not shown).

To expand the above findings, we measured the level of p-FOXM1, FOXM1, cyclin E1, and CDK2 in primary epithelial ovarian cancer (EOC) tumor samples. All proteins were expressed, but with variable levels in tumors. We further determined the correlations between individual proteins. Notably, all of these related proteins significantly correlated with each other. The strongest correlations were found between CDK2 and cyclin E1, followed by p-FOXM1 and CDK2 and p-FOXM1 and cyclin E1. These results support that p-FOXM1 is strongly dependent on cyclin E1 and CDK2 levels, and that cyclin E1 levels are correlated with CDK2 levels, which is expected as the two proteins form a complex. To fully understand the significance of the correlations, further investigation into the EOC samples is needed. Western blotting and subsequent Spearman correlation analysis for non-related or antagonistic proteins, such as different CDKs or FOX family members, will help to place the observed correlations into better context.

Of the CDK inhibitors used, dinaciclib treatment caused the greatest decrease in p-FOXM1 levels in engineered FT282 cells; therefore we tested its ability to reduce p-FOXM1 in HGSC cells. As an experimental model, we used OVCAR8 HGSC cells, which displayed very high levels of p-FOXM1 among a panel of HGSC cell lines.

Dinaciclib treatment significantly decreased the amount of p-FOXM1 and CDK2 in the nuclear extracts from OVCAR8 cells. The effect that the other CDK inhibitors may have on p-FOXM1 in HGSC cell lines should be investigated in future studies. In addition, the effect of dinaciclib on p-FOXM1 in other HGSC cell lines should be assessed.

The diminution of CDK2 nuclear protein levels in OVCAR8 cells after dinaciclib treatment is interesting and suggests that inhibition of a CDK results in a decrease in its nuclear concentration, which warrants further investigation. Looking at the nuclear versus cytoplasmic levels of CDK1 and 2 in the nuclear and cytoplasmic extracts of FT282 cell lines, and in additional HGSC cell lines treated with dinaciclib, will help reveal the significance of the above observation. It is plausible that dinaciclib works not only by inhibiting CDK enzymatic activity but also by leading to the degradation of CDK2 or by causing a decrease of its transport into the nucleus.

Dinaciclib, with its effects seen in both the FT282 and HGSC cell models, has shown encouraging results blocking phosphorylation of FOXM1 and thus, preventing the activation of FOXM1. This, combined with its use in cancer clinical trials, suggests that it has potential as a therapeutic agent in *CCNE1* amplified HGSC (124). More inquiries into dinaciclib effects in HGSC are needed, such as treatments at varying timepoints, to observe its impact on FOXM1 phosphorylation over time. In addition, whether the biological effects of dinaciclib in HGSC are related to its impact on FOXM1 phosphorylation should be determined.

Conversely, R03306 may also be an intriguing prospect in treating HGSC. As shown here, R03306 treatment increases the levels of p-FOXM1, indicating that a compensatory mechanism continues phosphorylating FOXM1 in the absence of CDK1 activity. Interestingly, too much p-FOXM1 could prove to be deleterious to the cell, by pushing cells through the cell cycle inappropriately and inducing mitotic catastrophe. Mitotic catastrophe is a result of aberrant mitosis and leads to cell death through

apoptosis or necrosis (125). Thus, treatment with R03306 and subsequent induction of p-FOXM1 could result in mitotic catastrophe of cancer cells, as they progress through the cell cycle improperly.

Phenotypic assays were performed to investigate the role of CCNE1 and FOXM1 in FTE cellular transformation. Ectopic expression of CCNE1 and FOXM1 in FT282 cells promoted an increase in cellular proliferation, migration, and invasion in comparison to the vector control and singly expressing FT282 cell lines. However, unlike the other transformation phenotypes, the E1/F1 FT282 overexpressing line did not show increased colony formation compared to single ectopic expression cell lines, suggesting the mechanisms involved in this particular phenotype are distinct.

These data underscore that CCNE1 and FOXM1, as well as cyclin E1 dependent phosphorylation of FOXM1, plays a role in FTE cell proliferation, invasion, and migration, but are not as integral in colony formation. Interestingly, FOXM1 seems to be important in invasion and migration, which is consistent with our unpublished observations of the gene expression signatures in FT282 cells engineered for dual E1/F1 ectopic expression. This is an important observation, as invasion and subsequent metastasis account for 90% of mortality in solid cancers. There are classes of anti-invasion treatments, such as matrix metalloprotease inhibitors and drugs targeting actin and myosin, which could show promise in HGSC, as FOXM1 is a major contributor to these processes (126).

In summary, we have investigated the interplay between FOXM1 and CCNE1 using FTE and HGSC models. We show for the first time that cyclin E1 promotes the phosphorylation of FOXM1 in HGSC, and show that this event is likely relevant both *in vitro* and *in vivo*. We also provide evidence that CDK2 is the key kinase that complexes with CCNE1 to mediate p-FOXM1 at residue threonine 600. Importantly, we demonstrate that FOXM1 and CCNE1 work together to drive critical transformation

phenotypes, including migration and invasion. Future studies will examine the importance of the functional interactions of FOXM1, cyclin E1, and CDK2 in HGSC biology and treatment.

LITERATURE CITED

1. National Cancer Institute. Cancer stat facts: ovarian cancer. https://seer.cancer.gov/statfacts/html/ovary.html. 2020. Accessed June 2020.
2. Siegel R, Ma J, Zou Z, Jemal A. Cancer statistics, 2014. CA: a cancer journal for clinicians **2014**;64:9-29.
3. Torre L, Trabert B, DeSantis C, Miller, K., Samimi G, Runowicz C., Gaudet M., Jemal A, Siegel L. Ovarian cancer statistics, 2018. CA: a cancer journal for clinicians **2018**;68(4): 284–296.
4. Serov SF, Scully RE, Sobin LH. Histological typing of ovarian tumors. Geneva: World Health Organization 1973.
5. Scully R, Xobin L. Histological typing of ovarian tumours. New York: Springer Berlin 1999.
6. Vaughan S, Coward JI, Bast RC, Jr., Berchuck A, Berek JS, Brenton JD*, et al.* Rethinking ovarian cancer: recommendations for improving outcomes. Nat Rev Cancer **2011**;11:719-25
7. Prat J. Staging classification for cancer of the ovary, fallopian tube, and peritoneum. International journal of gynaecology and obstetrics: the official organ of the International Federation of Gynaecology and Obstetrics **2014**;124:1-5.
8. Vaughan S, Coward JI, Bast RC, Berchuck A, Berek JS, Brenton JD, Coukos G, Crum CC, Drapkin R, Etemadmoghadam D, Friedlander M. Rethinking ovarian cancer: recommendations for improving outcomes. Nature Reviews Cancer **2011**;11(10):719-25.
9. Reid BM, Permuth JB, Sellers TA. Epidemiology of ovarian cancer: a review. Cancer biology & medicine **2017**;14(1):9.
10. Roett MA, Evans P. Ovarian cancer: an overview. American family physician **2009**;80:609-16.
11. Drake J. Diagnosis and management of the adnexal mass. American family physician **1998**;57:2471-6, 9-80.
12. Bast RC, Feeney MA, Lazarus HE, Nadler LM, Colvin RB, Knapp RC. Reactivity of a monoclonal antibody with human ovarian carcinoma. The Journal of clinical investigation. **1981**;68(5):1331-7.
13. Bast RC, Feeney MA, Lazarus HE, Nadler LM, Colvin RB, Knapp RC. Reactivity of a monoclonal antibody with human ovarian carcinoma. The Journal of clinical investigation. **1981**;68(5):1331-7.
14. Nebgen DR, Lu KH, Bast RC. Novel Approaches to Ovarian Cancer Screening. Current oncology reports. 2019 Aug 1;21(8):75.
15. Drapkin R, Von Horsten HH, Lin Y, Mok SC, Crum CP, Welch WR, Hecht JL. Human epididymis protein 4 (HE4) is a secreted glycoprotein that is overexpressed by serous and endometrioid ovarian carcinomas. Cancer research. **2005**;65(6):2162-9.
16. Dochez V, Caillon H, Vaucel E, Dimet J, Winer N, Ducarme G. Biomarkers and algorithms for diagnosis of ovarian cancer: CA125, HE4, RMI and ROMA, a review. Journal of ovarian research. **2019**;12(1):28.
17. Andersen MR, Goff BA, Lowe KA, Scholler N, Bergan L, Drescher CW, Paley P, Urban N. Use of a Symptom Index, CA125, and HE4 to predict ovarian cancer. Gynecologic oncology. **2010**;116(3):378-83.
18. Benedet JL, Bender H, Jones H, 3rd, Ngan HY, Pecorelli S. FIGO staging classifications and clinical practice guidelines in the management of gynecologic cancers. FIGO Committee on Gynecologic Oncology.

International journal of gynaecology and obstetrics: the official organ of the International Federation of Gynaecology and Obstetrics **2000**;70:209-62).
19. Cho KR, Shih Ie M. Ovarian cancer. Annual review of pathology **2009**;4:287-313.
20. Romero I, Bast RC, Jr. Minireview: human ovarian cancer: biology, current management, and paths to personalizing therapy. Endocrinology **2012**;153:1593-602.
21. Chen S, Parmigiani G. Meta-analysis of BRCA1 and BRCA2 penetrance. Journal of clinical oncology: official journal of the American Society of Clinical Oncology. **2007**;25(11):1329.
22. Møller P, Seppälä T, Bernstein I, Holinski-Feder E, Sala P, Evans DG, Lindblom A, Macrae F, Blanco I, Sijmons R, Jeffries J. Cancer incidence and survival in Lynch syndrome patients receiving colonoscopic and gynaecological surveillance: first report from the prospective Lynch syndrome database. Gut. **2017**;66(3):464-72.).
23. Sung HK, Ma SH, Choi JY, Hwang Y, Ahn C, Kim BG, Kim YM, Kim JW, Kang S, Kim J, Kim TJ. The effect of breastfeeding duration and parity on the risk of epithelial ovarian cancer: a systematic review and meta-analysis. Journal of preventive medicine and public health. **2016**;49(6):349.
24. Havrilesky LJ, Moorman PG, Lowery WJ, Gierisch JM, Coeytaux RR, Urrutia RP, Dinan M, McBroom AJ, Hasselblad V, Sanders GD, Myers ER. Oral contraceptive pills as primary prevention for ovarian cancer: a systematic review and meta-analysis. Obstetrics & Gynecology. **2013**;122(1):139-47.
25. Cibula D, Widschwendter M, Majek O, Dusek L. Tubal ligation and the risk of ovarian cancer: review and meta-analysis. Human reproduction update. **2011**;17(1):55-67.
26. Fathalla MF. Incessant ovulation--a factor in ovarian neoplasia? Lancet **1971**;2:163.
27. Piek JM, van Diest PJ, Zweemer RP, Jansen JW, Poort-Keesom RJ, Menko FH*, et al.* Dysplastic changes in prophylactically removed Fallopian tubes of women predisposed to developing ovarian cancer. J Pathol **2001**;195:451-6.
28. O'Shannessy DJ, Jackson SM, Twine NC, Hoffman BE, Dezso Z, Agoulnik SI*, et al.* Gene expression analyses support fallopian tube epithelium as the cell of origin of epithelial ovarian cancer. International journal of molecular sciences **2013**;14:13687-703.
29. Klinkebiel D, Zhang W, Akers SN, Odunsi K, Karpf AR. DNA Methylome Analyses Implicate Fallopian Tube Epithelia as the Origin for High-Grade Serous Ovarian Cancer. Mol Cancer Res **2016**;14:787-94.
30. Lee Y, Miron A, Drapkin R, Nucci MR, Medeiros F, Saleemuddin A, Garber J, Birch C, Mou H, Gordon RW, Cramer DW. A candidate precursor to serous carcinoma that originates in the distal fallopian tube. The Journal of Pathology: A Journal of the Pathological Society of Great Britain and Ireland. **2007**;211(1):26-35.
31. Soong TR, Howitt BE, Horowitz N, Nucci MR, Crum CP. The fallopian tube,“precursor escape” and narrowing the knowledge gap to the origins of high-grade serous carcinoma. Gynecologic oncology. 2019 Feb 1;152(2):426-33.
32. Perets R, Wyant GA, Muto KW, Bijron JG, Poole BB, Chin KT, Chen JY, Ohman AW, Stepule CD, Kwak S, Karst AM. Transformation of the fallopian tube secretory epithelium leads to high-grade serous ovarian cancer in Brca; Tp53; Pten models. Cancer cell. **2013**;24(6):751-65.

33. Kim J, Coffey DM, Creighton CJ, Yu Z, Hawkins SM, Matzuk MM. High-grade serous ovarian cancer arises from fallopian tube in a mouse model. Proceedings of the National Academy of Sciences. **2012**;109(10):3921-6.
34. Zhang S, Dolgalev I, Zhang T, Ran H, Levine DA, Neel BG. Both fallopian tube and ovarian surface epithelium are cells-of-origin for high-grade serous ovarian carcinoma. Nature communications. **2019**;10(1):1-6.
35. Network CGA. Comprehensive molecular portraits of human breast tumours. Nature **2012**;490:61-70.
36. Cancer Genome Atlas Research N. Integrated genomic analyses of ovarian carcinoma. Nature **2011**;474:609-15.
37. Ciriello G, Miller ML, Aksoy BA, Senbabaoglu Y, Schultz N, Sander C. Emerging landscape of oncogenic signatures across human cancers. Nature genetics **2013**;45:1127-33.
38. Etemadmoghadam D, Weir BA, Au-Yeung G, Alsop K, Mitchell G, George J*, et al.* Synthetic lethality between CCNE1 amplification and loss of BRCA1. Proc Natl Acad Sci U S A **2013**;110:19489-94.
39. Karst AM, Jones PM, Vena N, Ligon AH, Liu JF, Hirsch MS, Etemadmoghadam D, Bowtell DD, Drapkin R. Cyclin E1 deregulation occurs early in secretory cell transformation to promote formation of fallopian tube–derived high-grade serous ovarian cancers. Cancer research. **2014**;74(4):1141-52.
40. Barger CJ, Zhang W, Hillman J, Stablewski AB, Higgins MJ, Vanderhyden BC*, et al.* Genetic determinants of FOXM1 ectopic expression in epithelial ovarian cancer and functional contribution to cell cycle progression. Oncotarget **2015**;6:27613-27.
41. Gentles AJ, Newman AM, Liu CL, Bratman SV, Feng W, Kim D*, et al.* The prognostic landscape of genes and infiltrating immune cells across human cancers. Nat Med **2015**;21:938-45.
42. Dai J, Yang L, Wang J, Xiao Y, Ruan Q. Prognostic Value of FOXM1 in Patients with Malignant Solid Tumor: A Meta-Analysis and System Review. Dis Markers **2015**;2015:352478.
43. Barger CJ, Branick C, Chee L, Karpf AR. Pan-cancer analyses reveal genomic features of FOXM1 ectopic expression in cancer. Cancers. **2019**;11(2):251.
44. Bowtell DD, Bohm S, Ahmed AA, Aspuria PJ, Bast RC, Jr., Beral V*, et al.* Rethinking ovarian cancer II: reducing mortality from high-grade serous ovarian cancer. Nat Rev Cancer **2015**;15:668.
45. Bowtell DD. The genesis and evolution of high-grade serous ovarian cancer. Nat Rev Cancer **2010**;10:803-8
46. Cooke SL, Brenton JD. Evolution of platinum resistance in high-grade serous ovarian cancer. The lancet oncology. **2011**;12(12):1169-74.
47. Farmer H, McCabe N, Lord CJ, Tutt AN, Johnson DA, Richardson TB*, et al.* Targeting the DNA repair defect in BRCA mutant cells as a therapeutic strategy. Nature **2005**;434:917-21.
48. Kaelin WG. The concept of synthetic lethality in the context of anticancer therapy. Nat Rev Cancer **2005**;5:689-98.
49. Audeh MW, Carmichael J, Penson RT, Friedlander M, Powell B, Bell-McGuinn KM*, et al.* Oral poly(ADP-ribose) polymerase inhibitor olaparib in patients with BRCA1 or BRCA2 mutations and recurrent ovarian cancer: a proof-of-concept trial. Lancet **2010**;376:245-51.
50. Fong PC, Boss DS, Yap TA, Tutt A, Wu P, Mergui-Roelvink M*, et al.* Inhibition of poly(ADP-ribose) polymerase in tumors from BRCA mutation

carriers. N Engl J Med **2009**;361:123-34.
51. Ledermann J, Harter P, Gourley C, Friedlander M, Vergote I, Rustin G*, et al.* Olaparib maintenance therapy in platinum-sensitive relapsed ovarian cancer. N Engl J Med **2012**;366:1382-92.
52. Kaufman B, Shapira-Frommer R, Schmutzler RK, Audeh MW, Friedlander M, Balmaña J*, et al.* Olaparib monotherapy in patients with advanced cancer and a germline BRCA1/2 mutation. J Clin Oncol **2015**;33:244-50.
53. Kim G, Ison G, McKee AE, Zhang H, Tang S, Gwise T*, et al.* FDA Approval Summary: Olaparib Monotherapy in Patients with Deleterious Germline BRCA-Mutated Advanced Ovarian Cancer Treated with Three or More Lines of Chemotherapy. Clin Cancer Res **2015**;21:4257-61.
54. Lord CJ, Tutt AN, Ashworth A. Synthetic lethality and cancer therapy: lessons learned from the development of PARP inhibitors. Annu Rev Med **2015**;66:455-70.
55. Bitler BG, Watson ZL, Wheeler LJ, Behbakht K. PARP inhibitors: Clinical utility and possibilities of overcoming resistance. Gynecol Oncol **2017**;147:695-704.
56. Fojo T, Bates S. Mechanisms of resistance to PARP inhibitors--three and counting. Cancer Discov **2013**;3:20-3.
57. Sonnenblick A, de Azambuja E, Azim HA, Piccart M. An update on PARP inhibitors--moving to the adjuvant setting. Nat Rev Clin Oncol **2015**;12:27-41.
58. Korver W, Roose J, Clevers H. The winged-helix transcription factor Trident is expressed in cycling cells. Nucleic Acids Res **1997**;25:1715-9.
59. Myatt SS, Lam EW. The emerging roles of forkhead box (Fox) proteins in cancer. Nature reviews Cancer **2007**;7:847-59.
60. Wierstra I, Alves J. Despite its strong transactivation domain, transcription factor FOXM1c is kept almost inactive by two different inhibitory domains. Biol Chem **2006**;387:963-76.
61. Park HJ, Wang Z, Costa RH, Tyner A, Lau LF, Raychaudhuri P. An N-terminal inhibitory domain modulates activity of FoxM1 during cell cycle. Oncogene. **2008**;27:1696–704.
62. Liao GB, Li XZ, Zeng S, Liu C, Yang SM, Yang L, Hu CJ, Bai JY. Regulation of the master regulator FOXM1 in cancer. Cell Communication and Signaling. **2018**;16(1):1-5.
63. Zhang X, Zhang L, Du Y, Zheng H, Zhang P, Sun Y, Wang Y, Chen J, Ding P, Wang N, Yang C. A novel FOXM1 isoform, FOXM1D, promotes epithelial–mesenchymal transition and metastasis through ROCKs activation in colorectal cancer. Oncogene. **2017**;36(6):807-19
64. Ma RY, Tong TH, Cheung AM, Tsang AC, Leung WY, Yao KM. Raf/MEK/MAPK signaling stimulates the nuclear translocation and transactivating activity of FOXM1c. Journal of cell science. **2005**;118(4):795-806.
65. Lüscher-Firzlaff JM, Lilischkis R, Lüscher B. Regulation of the transcription factor FOXM1c by Cyclin E/CDK2. FEBS letters. **2006**;580(7):1716-22.
66. Laoukili J, Alvarez M, Meijer LA, Stahl M, Mohammed S, Kleij L, Heck AJ, Medema RH. Activation of FoxM1 during G2 requires cyclin A/Cdk-dependent relief of autorepression by the FoxM1 N-terminal domain. Molecular and cellular biology. **2008**;28(9):3076-87
67. Xu K, Liu X, Mao X, Xue L, Wang R, Chen L, Chu X. MicroRNA-149 suppresses colorectal cancer cell migration and invasion by directly targeting

forkhead box transcription factor FOXM1. Cellular Physiology and Biochemistry. **2015**;35(2):499-515.
68. Liu X, Xie T, Mao X, Xue L, Chu X, Chen L. MicroRNA-149 increases the sensitivity of colorectal cancer cells to 5-fluorouracil by targeting forkhead box transcription factor FOXM1. Cellular physiology and biochemistry. **2016**;39(2):617-29.
69. Ke Y, Zhao W, Xiong J, Cao R. miR-149 inhibits non-small-cell lung cancer cells EMT by targeting FOXM1. Biochemistry research international. **2013**.
70. Westendorf JM, Rao PN, Gerace L. Cloning of cDNAs for M-phase phosphoproteins recognized by the MPM2 monoclonal antibody and determination of the phosphorylated epitope. Proc Natl Acad Sci U S A **1994**;91:714-8.
71. Wang IC, Chen YJ, Hughes D, Petrovic V, Major ML, Park HJ*, et al.* Forkhead box M1 regulates the transcriptional network of genes essential for mitotic progression and genes encoding the SCF (Skp2-Cks1) ubiquitin ligase. Mol Cell Biol **2005**;25:10875-94.
72. Wonsey DR, Follettie MT. Loss of the forkhead transcription factor FoxM1 causes centrosome amplification and mitotic catastrophe. Cancer Res **2005**;65:5181-9.
73. Laoukili J, Kooistra MR, Bras A, Kauw J, Kerkhoven RM, Morrison A*, et al.* FoxM1 is required for execution of the mitotic programme and chromosome stability. Nat Cell Biol **2005**;7:126-36.
74. Krupczak-Hollis K, Wang X, Kalinichenko VV, Gusarova GA, Wang IC, Dennewitz MB*, et al.* The mouse Forkhead Box m1 transcription factor is essential for hepatoblast mitosis and development of intrahepatic bile ducts and vessels during liver morphogenesis. Dev Biol **2004**;276:74-88.
75. Wang, Costa RH. FoxM1 dances with mitosis. Nat Cell Biol **2005**;7:108-10.
76. Laoukili J, Alvarez-Fernandez M, Stahl M, Medema RH. FoxM1 is degraded at mitotic exit in a Cdh1-dependent manner. Cell Cycle **2008**;7:2720-6.
77. Halasi M, Gartel AL. FOX(M1) news--it is cancer. Molecular cancer therapeutics **2013**;12:245-54.
78. Tan Y, Raychaudhuri P, Costa RH. Chk2 mediates stabilization of the FoxM1 transcription factor to stimulate expression of DNA repair genes. Molecular and cellular biology. **2007**;27(3):1007-16.
79. Wang Z, Banerjee S, Kong D, Li Y, Sarkar FH. Down-regulation of Forkhead Box M1 transcription factor leads to the inhibition of invasion and angiogenesis of pancreatic cancer cells. Cancer research. **2007**;67(17):8293-300.
80. Chiu WT, Huang YF, Tsai HY, Chen CC, Chang CH, Huang SC, Hsu KF, Chou CY. FOXM1 confers to epithelial-mesenchymal transition, stemness and chemoresistance in epithelial ovarian carcinoma cells. Oncotarget. **2015**;6(4):2349.
81. Pandit B, Halasi M, Gartel AL. p53 negatively regulates expression of FoxM1. Cell cycle **2009**;8:3425-7.
82. Barsotti AM, Prives C. Pro-proliferative FoxM1 is a target of p53-mediated repression. Oncogene **2009**;28:4295-305.
83. Levanon K, Sapoznik S, Bahar-Shany K, Brand H, Shapira-Frommer R, Korach J*, et al.* FOXO3a loss is a frequent early event in high-grade pelvic serous carcinogenesis. Oncogene **2014**;33:4424-32.
84. McGovern UB, Francis RE, Peck B, Guest SK, Wang J, Myatt SS*, et al.* Gefitinib (Iressa) represses FOXM1 expression via FOXO3a in breast cancer.

Molecular cancer therapeutics **2009**;8:582-91.
85. Blanco-Bose WE, Murphy MJ, Ehninger A, Offner S, Dubey C, Huang W*, et al.* C-Myc and its target FoxM1 are critical downstream effectors of constitutive androstane receptor (CAR) mediated direct liver hyperplasia. Hepatology **2008**;48:1302-11.
86. Mencalha AL, Binato R, Ferreira GM, Du Rocher B, Abdelhay E. Forkhead box M1 (FoxM1) gene is a new STAT3 transcriptional factor target and is essential for proliferation, survival and DNA repair of K562 cell line. PloS one **2012**;7:e48160.
87. Teh MT, Wong ST, Neill GW, Ghali LR, Philpott MP, Quinn AG. FOXM1 is a downstream target of Gli1 in basal cell carcinomas. Cancer research **2002**;62:4773-80.
88. Kong X, Li L, Li Z, Le X, Huang C, Jia Z*, et al.* Dysregulated expression of FOXM1 isoforms drives progression of pancreatic cancer. Cancer research **2013**;73:3987-96.
89. Xia LM, Huang WJ, Wang B, Liu M, Zhang Q, Yan W*, et al.* Transcriptional up-regulation of FoxM1 in response to hypoxia is mediated by HIF-1. J Cell Biochem **2009**;106:247-56.
90. Millour J, de Olano N, Horimoto Y, Monteiro LJ, Langer JK, Aligue R*, et al.* ATM and p53 regulate FOXM1 expression via E2F in breast cancer epirubicin treatment and resistance. Molecular cancer therapeutics **2011**;10:1046-58.
91. Kalin TV, Ustiyan V, Kalinichenko VV. Multiple faces of FoxM1 transcription factor: lessons from transgenic mouse models. Cell Cycle **2011**;10:396-405).
92. Barger et al., in preparation.
93. Lew DJ, Dulić V, Reed SI. Isolation of three novel human cyclins by rescue of G1 cyclin (Cln) function in yeast. Cell. 1**991**;66(6):1197-206.
94. Murray AW. Recycling the cell cycle: cyclins revisited. Cell. **2004**;116(2):221-34.
95. Bernheim A. Cytogenomics of cancers: From chromosome to sequence. Molecular oncology. **2010**;4(4):309-22.
96. Keyomarsi K, Akli S. Cyclin E and its low molecular weight forms in human cancer and as targets for cancer therapy. Cancer biology and therapy. 2003;2(4):S38-47.
97. Honda R, Lowe ED, Dubinina E, Skamnaki V, Cook A, Brown NR, Johnson LN. The structure of cyclin E1/CDK2: implications for CDK2 activation and CDK2-independent roles. The EMBO journal. **2005**;24(3):452-63.
98. Caldon CE, Musgrove EA. Distinct and redundant functions of cyclin E1 and cyclin E2 in development and cancer. Cell division. **2010**;5(1):1-3.
99. Koff A, Giordano A, Desai D, Yamashita K, Harper JW, Elledge S, Nishimoto T, Morgan DO, Franza BR, Roberts JM. Formation and activation of a cyclin E-cdk2 complex during the G1 phase of the human cell cycle. Science. **1992**;257(5077):1689-94.
100. Ohtsubo M, Theodoras AM, Schumacher J, Roberts JM, Pagano M. Human cyclin E, a nuclear protein essential for the G1-to-S phase transition. Molecular and cellular biology. **1995**;15(5):2612-24.
101. Geng Y, Eaton EN, Picon M, Roberts JM, Lundberg AS, Gifford A, Sardet C, Weinberg RA. Regulation of cyclin E transcription by E2Fs and retinoblastoma protein. Oncogene. **1996;**12(6):1173-80.
102. Santoni-Rugiu E, Falck J, Mailand N, Bartek J, Lukas J. Involvement of Myc activity in a G1/S-promoting mechanism parallel to the pRb/E2F pathway. Molecular and cellular biology. **2000**;20(10):3497-509.

103. Aleem E, Kiyokawa H, Kaldis P. Cdc2–cyclin E complexes regulate the G1/S phase transition. Nature cell biology. **2005**;7(8):831-6.
104. Geng Y, Lee YM, Welcker M, Swanger J, Zagozdzon A, Winer JD, Roberts JM, Kaldis P, Clurman BE, Sicinski P. Kinase-independent function of cyclin E. Molecular cell. **2007**;25(1):127-39.
105. Kanska J, Zakhour M, Taylor-Harding B, Karlan BY, Wiedemeyer WR. Cyclin E as a potential therapeutic target in high-grade serous ovarian cancer. Gynecologic oncology. **2016**;143(1):152-8.
106. Bedrosian I, Lu KH, Verschraegen C, Keyomarsi K. Cyclin E deregulation alters the biologic properties of ovarian cancer cells. Oncogene. **2004**;23(15):2648-57.
107. Ekholm-Reed S, Méndez J, Tedesco D, Zetterberg A, Stillman B, Reed SI. Deregulation of cyclin E in human cells interferes with prereplication complex assembly. The Journal of cell biology. **2004**;165(6):789-800.
108. Kawamura K, Izumi H, Ma Z, Ikeda R, Moriyama M, Tanaka T, Nojima T, Levin LS, Fujikawa-Yamamoto K, Suzuki K, Fukasawa K. Induction of centrosome amplification and chromosome instability in human bladder cancer cells by p53 mutation and cyclin E overexpression. Cancer research. **2004**;64(14):4800-9.
109. Nakayama N, Nakayama K, Shamima Y, Ishikawa M, Katagiri A, Iida K, Miyazaki K. Gene amplification CCNE1 is related to poor survival and potential therapeutic target in ovarian cancer. Cancer: Interdisciplinary International Journal of the American Cancer Society. **2010**;116(11):2621-34.
110. Caruso JA, Duong MT, Carey JP, Hunt KK, Keyomarsi K. Low-molecular-weight cyclin E in human Cancer: cellular consequences and opportunities for targeted therapies. Cancer research. **2018**;78(19):5481-91.
111. Karst AM, Drapkin R. Primary culture and immortalization of human fallopian tube secretory epithelial cells. Nat Protoc **2012**;7:1755-64
112. Barger CJ, Zhang W, Sharma A, Chee L, James SR, Kufel CN, Miller A, Meza J, Drapkin R, Odunsi K, Klinkebiel D. Expression of the POTE gene family in human ovarian cancer. Scientific reports. **2018**;8(1):1-3
113. Paruch K, Dwyer MP, Alvarez C, Brown C, Chan TY, Doll RJ, Keertikar K, Knutson C, McKittrick B, Rivera J, Rossman R. Discovery of dinaciclib (SCH 727965): a potent and selective inhibitor of cyclin-dependent kinases. ACS medicinal chemistry letters. **2010**;1(5):204-8.
114. Parry D, Guzi T, Shanahan F, Davis N, Prabhavalkar D, Wiswell D, Seghezzi W, Paruch K, Dwyer MP, Doll R, Nomeir A. Dinaciclib (SCH 727965), a novel and potent cyclin-dependent kinase inhibitor. Molecular cancer therapeutics. **2010**;9(8):2344-53.
115. Vassilev LT, Tovar C, Chen S, Knezevic D, Zhao X, Sun H, Heimbrook DC, Chen L. Selective small-molecule inhibitor reveals critical mitotic functions of human CDK1. Proceedings of the National Academy of Sciences. **2006**;103(28):10660-5
116. Toogood PL, Harvey PJ, Repine JT, Sheehan DJ, VanderWel SN, Zhou H, Keller PR, McNamara DJ, Sherry D, Zhu T, Brodfuehrer J. Discovery of a potent and selective inhibitor of cyclin-dependent kinase 4/6. Journal of medicinal chemistry. **2005**;48(7):2388-406.
117. Wyatt PG, Woodhead AJ, Berdini V, Boulstridge JA, Carr MG, Cross DM, Davis DJ, Devine LA, Early TR, Feltell RE, Lewis EJ. Identification of N-(4-piperidinyl)-4-(2, 6-dichlorobenzoylamino)-1 H-pyrazole-3-carboxamide (AT7519), a novel cyclin dependent kinase inhibitor using fragment-based X-

ray crystallography and structure based drug design. Journal of medicinal chemistry. **2008**;51(16):4986-99.
118. Squires MS, Feltell RE, Wallis NG, Lewis EJ, Smith DM, Cross DM, Lyons JF, Thompson NT. Biological characterization of AT7519, a small-molecule inhibitor of cyclin-dependent kinases, in human tumor cell lines. Molecular cancer therapeutics. **2009**;8(2):324-32
119. Mermel CH, Schumacher SE, Hill B, Meyerson ML, Beroukhim R, Getz G. GISTIC2. 0 facilitates sensitive and confident localization of the targets of focal somatic copy-number alteration in human cancers. Genome biology. **2011**;12(4):R41.
120. Yang L, Fang D, Chen H, Lu Y, Dong Z, Ding HF, Jing Q, Su SB, Huang S. Cyclin-dependent kinase 2 is an ideal target for ovary tumors with elevated cyclin E1 expression. Oncotarget. **2015**;6(25):20801
121. Mita MM, Joy AA, Mita A, Sankhala K, Jou YM, Zhang D, Statkevich P, Zhu Y, Yao SL, Small K, Bannerji R. Randomized phase II trial of the cyclin-dependent kinase inhibitor dinaciclib (MK-7965) versus capecitabine in patients with advanced breast cancer. Clinical breast cancer. 2014 Jun 1;14(3):169-76.
122. Stephenson JJ, Nemunaitis J, Joy AA, Martin JC, Jou YM, Zhang D, Statkevich P, Yao SL, Zhu Y, Zhou H, Small K. Randomized phase 2 study of the cyclin-dependent kinase inhibitor dinaciclib (MK-7965) versus erlotinib in patients with non-small cell lung cancer. Lung cancer. **2014**;83(2):219-23.
123. Kumar SK, LaPlant B, Chng WJ, Zonder J, Callander N, Fonseca R, Fruth B, Roy V, Erlichman C, Stewart AK. Dinaciclib, a novel CDK inhibitor, demonstrates encouraging single-agent activity in patients with relapsed multiple myeloma. Blood. **2015**;125(3):443-8.
124. Etemadmoghadam D, Au-Yeung G, Wall M, Mitchell C, Kansara M, Loehrer E, Batzios C, George J, Ftouni S, Weir BA, Carter S. Resistance to CDK2 inhibitors is associated with selection of polyploid cells in CCNE1-amplified ovarian cancer. Clinical Cancer Research. **2013**;19(21):5960-71.
125. Vakifahmetoglu H, Olsson M, Zhivotovsky B. Death through a tragedy: mitotic catastrophe. Cell Death & Differentiation. **2008**;15(7):1153-62.
126. Gandalovičová A, Rosel D, Fernandes M, Veselý P, Heneberg P, Čermák V, Petruželka L, Kumar S, Sanz-Moreno V, Brábek J. Migrastatics—anti-metastatic and anti-invasion drugs: promises and challenges. Trends in cancer. **2017**;3(6):391-406.